

# WT1 Is Necessary for the Proliferation and Migration of Cells of Renin Lineage Following Kidney Podocyte Depletion

Natalya V. Kaverina,<sup>1</sup> Diana G. Eng,<sup>1</sup> Andrea D. Largent,<sup>1</sup> Ilse Daehn,<sup>2</sup> Anthony Chang,<sup>3</sup> Kenneth W. Gross,<sup>4</sup> Jeffrey W. Pippin,<sup>1</sup> Peter Hohenstein,<sup>5</sup> and Stuart J. Shankland<sup>1,\*</sup>

<sup>1</sup>Division of Nephrology, University of Washington School of Medicine, 750 Republican Street, Seattle, WA 98109, USA

<sup>2</sup>Department of Medicine, Division of Nephrology, The Icahn School of Medicine at Mount Sinai, 1468 Madison Avenue, New York, NY 10029, USA

<sup>3</sup>Department of Pathology, University of Chicago, 5841 S Maryland Ave, Chicago, IL 60637, USA

<sup>4</sup>Department of Molecular and Cellular Biology, Roswell Park Cancer Institute, Elm & Carlton Streets, Buffalo, NY 14263, USA

<sup>5</sup>The Roslin Institute, University of Edinburgh, Easter Bush, Midlothian EH25 9RG, UK

\*Correspondence: [stuartjs@uw.edu](mailto:stuartjs@uw.edu)

<http://dx.doi.org/10.1016/j.stemcr.2017.08.020>

## SUMMARY

Wilms' tumor suppressor 1 (WT1) plays an important role in cell proliferation and mesenchymal-epithelial balance in normal development and disease. Here, we show that following podocyte depletion in three experimental models, and in patients with focal segmental glomerulosclerosis (FSGS) and membranous nephropathy, WT1 increased significantly in cells of renin lineage (CoRL). In an animal model of FSGS in *RenWt1<sup>fl/fl</sup>* reporter mice with inducible deletion of WT1 in CoRL, CoRL proliferation and migration to the glomerulus was reduced, and glomerular disease was worse compared with wild-type mice. To become podocytes, CoRL undergo mesenchymal-to-epithelial transformation (MET), typified by reduced staining for mesenchymal markers (MYH11, SM22,  $\alpha$ SMA) and *de novo* expression of epithelial markers (E-cadherin and cytokeratin18). Evidence for changes in MET markers was barely detected in *RenWt1<sup>fl/fl</sup>* mice. Our results show that following podocyte depletion, WT1 plays essential roles in CoRL proliferation and migration toward an adult podocyte fate.

## INTRODUCTION

Kidney podocytes are terminally differentiated glomerular epithelial cells unable to self-renew due to their inability to proliferate (Lasagni et al., 2013; Wanner et al., 2014), and replacement following loss is dependent on local kidney progenitors (Ronconi et al., 2009; Lasagni et al., 2015; Starke et al., 2015). Glomerular parietal epithelial cells (PECs) (Romagnani, 2011; Zhang et al., 2013; Eng et al., 2015; Kuppe et al., 2015; Lazzeri and Romagnani, 2015) and cells of renin lineage (CoRL) (Pippin et al., 2013, 2014; Lichtnekert et al., 2016) are considered likely adult podocyte progenitors. CoRL serve as progenitors for several kidney cell types (Sequeira Lopez et al., 2004), including podocytes (Grahammer et al., 2013; Pippin et al., 2013, 2014, 2015; Shankland et al., 2014; Lichtnekert et al., 2016), PECs (Pippin et al., 2013; Eng et al., 2015), mesangial cells (Thoma, 2014; Starke et al., 2015), and pericytes (Stefanska et al., 2013; Pippin et al., 2015). RAAS inhibition augments the CoRL reservoir in the juxta-glomerular compartment (JGC) through proliferation, enhances migration to the glomerulus, and increases transdifferentiation toward a podocyte fate (Lichtnekert et al., 2016). CoRL and podocytes derive from mesenchymal origins (Costantini and Kopan, 2010; Matsushita et al., 2010; Little and McMahon, 2012; Wang et al., 2013). CoRL maintain mesenchymal characteristics, whereas adult podocytes exhibit epithelial characteristics (Filipovic et al., 2017). Therefore, for CoRL to serve as podocyte

progenitors, they must undergo changes resembling a mesenchymal-to-epithelial transition (MET).

The transcription factor Wilms' tumor suppressor protein 1 (WT1) is required for podocyte development and homeostasis (Kann et al., 2015). Missense mutations and conditionally deleting WT1 from podocytes leads to glomerular scarring in humans and mice (Pelletier et al., 1991; Gao et al., 2004; Chau et al., 2011). WT1 is closely linked to the mesenchymal-epithelial balance in development and disease (Miller-Hodges and Hohenstein, 2012), and the homeostasis of different cell types (Ozdemir and Hohenstein, 2014), including the plasticity and cell fate of certain cells (Karki et al., 2014; Wen et al., 2016). WT1 drives MET at the start of nephron development (Essafi et al., 2011; Berry et al., 2015), although in the developing epicardium, WT1 controls the reverse, i.e., epithelial-to-mesenchymal transition (Martinez-Estrada et al., 2010). WT1 enhances proliferation and migration in certain cell types in a context-dependent manner (Wagner et al., 2008; Brett et al., 2013; Graziano et al., 2017). Finally, WT1 and renin co-localize in a fraction of cells in the afferent arterioles. Moreover, WT1 (–KTS) can negatively modulate renin gene transcription through interaction at a binding site within the renin enhancer (Steege et al., 2008).

These reports provided the rationale to test the hypothesis that WT1 is required for CoRL proliferation, migration, and transdifferentiation toward a podocyte fate in the context of podocyte depletion.



**Cytotoxic Anti-Podocyte Antibody Model**  
**Wt1 Renin Collagen IV DAPI**

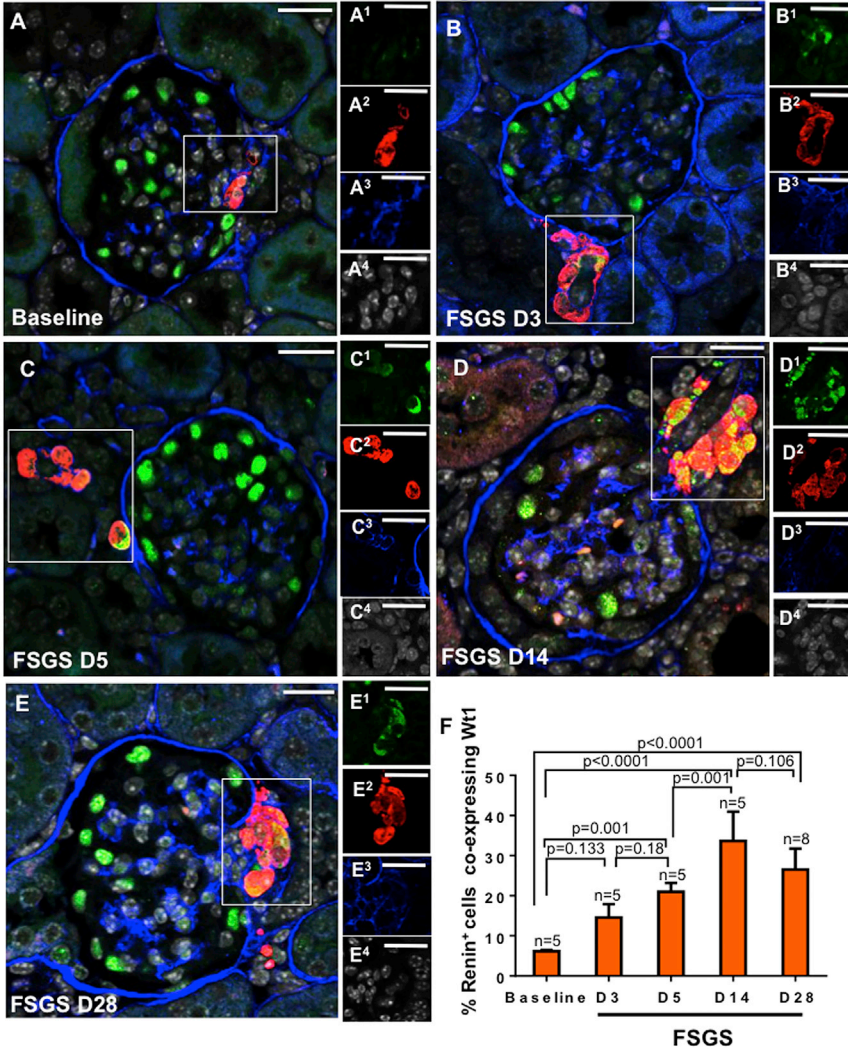


**Figure 1. WT1 Increases in Renin-Stained Cells in the Juxta-Glomerular Compartment Following Podocyte Depletion in the Cytotoxic Anti-podocyte Antibody Model of FSGS**

Confocal microscopy images marked (A–E) show the merge for WT1 (green), renin (red), collagen IV (blue), and DAPI (gray). Collagen IV demarcates glomeruli. Insets show the JGC for each channel, labeled as superscripts. Scale bars, 20  $\mu$ m.

(A) Baseline (n = 5), WT1 (A1) is limited to podocytes and not detected in renin-stained cells (A2).

(B) D3 (n = 5), WT1 (B1) is detected in the cytoplasm of renin-stained cells (B2).

(C) D5 (n = 5), WT1 (C1) increases in JGC, overlapping with renin (C2), creating a yellow color.

(D) D14 (n = 5), renin-stained cells (D2) co-staining with WT1 (D1) increase in the JGC.

(E) D28 (n = 8), WT1 (E1) and renin (E2) co-staining persists.

(F) Quantitation of the percentage of renin-stained cells in the JGC co-staining for WT1.

**RESULTS**

**WT1 Expression Increases in Renin-Stained Cells Following Podocyte Depletion in Mice and Humans**

We began by measuring the temporal expression of WT1 in renin-stained cells in the JGC in *RenWt1<sup>+/+</sup>* mice following podocyte depletion induced by the administration of a cytopathic anti-podocyte antibody. Following podocyte depletion, the percentage of renin cells co-staining for WT1 increased as follows (Figures 1A–1F): from a baseline to D3 of FSGS (6.16%  $\pm$  0.3% versus 14.5%  $\pm$  3.35%; p = 0.133; Figures 1A and 1B), from baseline to D5 of FSGS (6.16%  $\pm$  0.3% versus 20.99%  $\pm$  2.20%; p = 0.001; Figures 1A and 1C), from D5 to D14 of FSGS (20.99%  $\pm$  2.20% versus 33.63%  $\pm$  7.3%; p = 0.001; Figures 1C and 1D), and from baseline to

D28 of FSGS (6.16%  $\pm$  0.3% versus 26.5%  $\pm$  5.24%; p < 0.0001; Figures 1A and 1E).

Podocyte loss in podocyte TGF $\beta$ -Receptor1 transgenic (*PodTgfr1*) mice (Figures S1A–S1C) and membranous nephropathy rats (passive Heymann nephritis [PHN] model) (Figures S1D and S1E) was also accompanied by increased WT1 in renin-stained JGC cells. In contrast, WT1 was not detected in renin cells post uninephrectomy in mice, where absolute podocyte number remained normal (Figure S1F).

We confirmed the experimental results in human diseases. In normal human kidney, WT1 was mostly limited to podocytes (Figure 2A). However, *de novo* WT1 was detected in renin-stained JGC cells in human FSGS (Figure 2B) and membranous nephropathy (Figure 2C). Similar results were obtained with different WT1 antibodies, and no

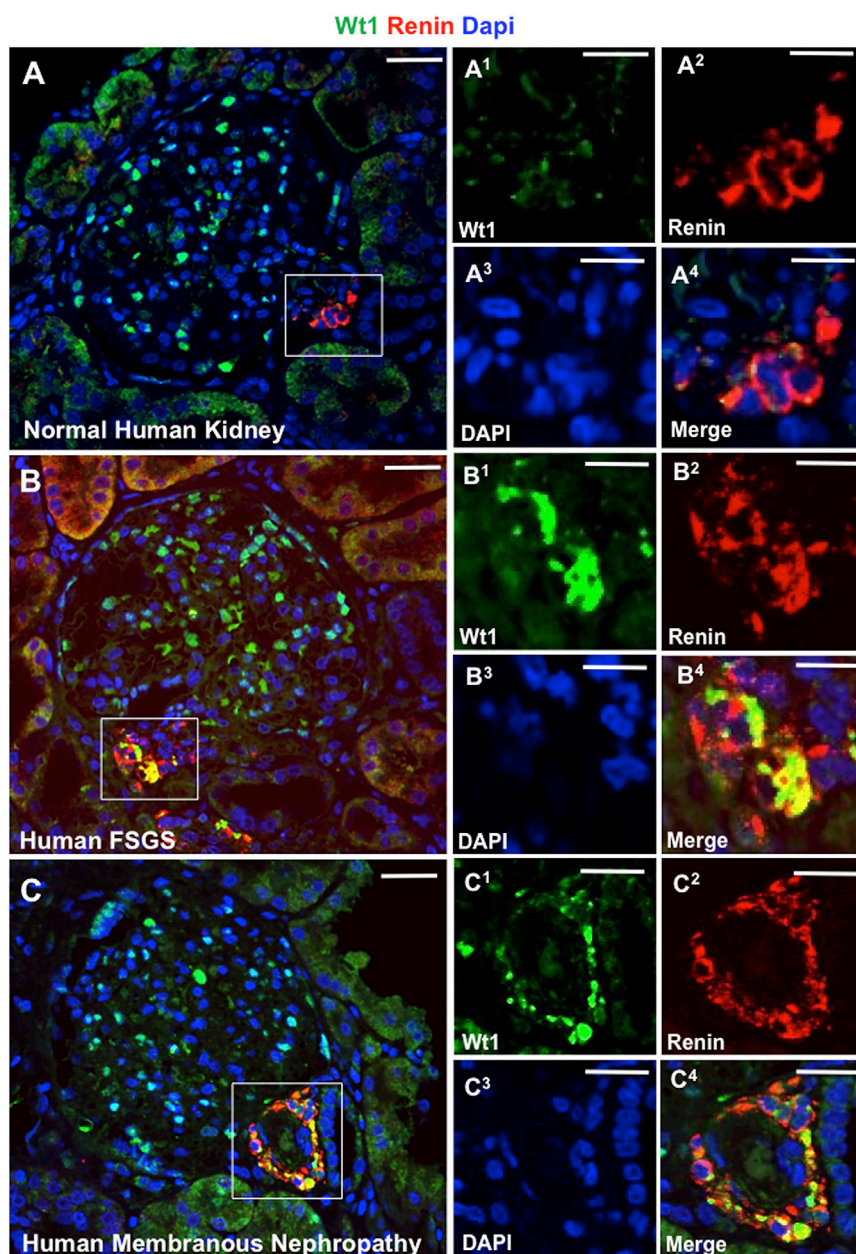


**Figure 2. WT1 Increases in Renin-Stained Cells in the JGC in Human FSGS and Membranous Nephropathy**

Confocal microscopy for WT1, renin, and DAPI in human kidneys. Insets show the JGC for each channel: WT1 (1, green), renin (2, red), DAPI (3, blue), and merged (4, yellow). Scale bars, 20  $\mu\text{m}$ .

(A) Normal human kidney ( $n = 5$ ), WT1 is limited to podocytes (A1), and not detected in renin-stained cells (A2), hence no merge (A4).

(B) Human FSGS ( $n = 5$ ), WT1 in the JGC (B1) overlaps with renin-stained cells (B2) creating a yellow color (B4).

(C) Human membranous nephropathy ( $n = 5$ ), WT1 (C1) and renin in the JGC (C2) produce a yellow color (C4).

staining was detected when the primary antibody was omitted (not shown).

These results show that WT1 protein increases in renin-stained cells in the JGC in both experimental and human FSGS and membranous nephropathy in the context of podocyte loss.

#### Selective Deletion of WT1 in Cells of Renin Lineage Has No Impact on Podocytes or Kidney Function under Non-diseased Conditions

To test if *de novo* expression of WT1 in CoRL has relevance for their progenitor role to replace lost podocytes, *RenCreER*

*tdTomato* mice (Pippin et al., 2013, 2015) were crossed with *Wt1<sup>fl/fl</sup>* mice (Martinez-Estrada et al., 2010; DeFilippis and Wagner, 2014) to generate *RenCreER tdTomato Wt1<sup>fl/fl</sup>* mice (abbreviated *RenWt1<sup>fl/fl</sup>*) so that WT1 could be conditionally and selectively deleted in tdTomato-labeled CoRL (Figure S2). CoRL and their descendants permanently express tdTomato dependent on Cre-mediated recombination, which allows lineage tracing of CoRL. Glomerular cells do not ectopically express renin (and hence Cre) under injury conditions. *RenCreER tdTomato Wt1<sup>+/+</sup>* (abbreviated *RenWt1<sup>+/+</sup>*) served as controls, where tdTomato was expressed in CoRL but WT1 remained (Figures S2A, S2E, and



S2H). Genotyping discerned the lox and wild-type *Wt1* alleles (Figure S2A1), and a flox deletion primer distinguished *RenWt1<sup>fl/fl</sup>* mice given tamoxifen versus corn oil (Figure S2A2). Following tamoxifen, *Wt1* mRNA from RFP<sup>+</sup>CoRL isolated using laser capture microscopy was significantly lower in *RenWt1<sup>fl/fl</sup>* compared with *RenWt1<sup>+/+</sup>* mice (Figure S2B), while *renin* mRNA levels were similar (Figure S2C). Cre was restricted to the JGC in mice containing the *CreER* transgene but not in Cre-negative mice (Figures S2D and S2E). TdTomato, detected without the use of an antibody, confirmed similar CoRL labeling efficiency in *RenWt1<sup>+/+</sup>* and *RenWt1<sup>fl/fl</sup>* mice given tamoxifen (Figures S2F and S2G). TdTomato was absent in *RenCre*-negative mice (not shown). Ninety-five percent of renin<sup>+</sup> CoRL stained with red fluorescent protein (RFP) antibody, which detected TdTomato in *RenWt1<sup>+/+</sup>* and *RenWt1<sup>fl/fl</sup>* mice (not shown). Mice that did not report were excluded, accounting for <1% of all mice given tamoxifen. At baseline, WT1 was in a typical podocyte distribution in *RenWt1<sup>fl/fl</sup>* mice, indistinguishable from *RenWt1<sup>+/+</sup>* mice, proving deletion in CoRL had no impact on podocytes (Figures S2H and S2I). WT1 was detected in <5% of CoRL in non-diseased *RenWt1<sup>+/+</sup>* mice but was not detected in CoRL in non-diseased *RenWt1<sup>fl/fl</sup>* mice (Figures S2H and S2I). These results show that *Wt1* mRNA and WT1 protein were selectively reduced in TdTomato<sup>+</sup> CoRL of *RenWt1<sup>fl/fl</sup>* but not in *RenWt1<sup>+/+</sup>* mice, with no consequences on podocyte health under normal conditions.

### Increased WT1 Was Not Seen in JGC of *Wt1* Conditional Knockout Mice Following Podocyte Depletion

WT1 overlap with RFP<sup>+</sup> was not present in the vast majority of CoRL in the JGC in normal *RenWt1<sup>+/+</sup>* and *RenWt1<sup>fl/fl</sup>* mice ( $7 \pm 2.5$  versus  $5.6 \pm 2.0$ , respectively;  $p = 0.99$ ; Figures 3A, 3D, and 3G). In *RenWt1<sup>+/+</sup>* mice at D28 following podocyte loss, RFP<sup>+</sup>CoRL in the JGC co-stained with WT1 increased compared with baseline ( $103 \pm 12.36$  versus  $7 \pm 2.5$ ;  $p < 0.001$ ; Figures 3B and 3G). By contrast, in *RenWt1<sup>fl/fl</sup>* mice at D28, only  $5.8 \pm 1.8$  of RFP<sup>+</sup> CoRL in the JGC co-stained with WT1 (Figures 3E and 3G). Because enalapril increases RFP<sup>+</sup>CoRL in the JGC (Lichtnekert et al., 2016), *RenWt1<sup>+/+</sup>* mice were given enalapril for 25 days following podocyte loss. RFP<sup>+</sup>CoRL in the JGC co-expressing WT1 further increased at D28 following enalapril compared with baseline ( $419.5 \pm 117.79$  versus  $7 \pm 2.5$ ;  $p < 0.0001$ ; Figures 3A, 3C, and 3G). An increase in WT1 expression was not observed in JGC of *RenWt1<sup>fl/fl</sup>* mice after enalapril (Figures 3F and 3G). Similarly, the number of RFP<sup>+</sup>WT1<sup>-</sup>CoRL increased in *RenWt1<sup>+/+</sup>* mice following podocyte depletion (Figures S3B, S3C), while the number of RFP<sup>+</sup>WT1<sup>-</sup>CoRL in *RenWt1<sup>fl/fl</sup>* mice did not increase (Figures S3E, S3F).

These results show the following: (1) although WT1 was not detected in the majority of cells in the JGC under normal conditions, the number of RFP<sup>+</sup>CoRL co-expressing WT1 increases progressively following podocyte loss in *RenWt1<sup>+/+</sup>* mice; (2) WT1 did not increase in RFP<sup>+</sup>CoRL in diseased *RenWt1<sup>fl/fl</sup>* mice, consistent with successful targeted ablation of WT1 in CoRL; (3) enalapril increased the number of CoRL co-expressing WT1 in *RenWt1<sup>+/+</sup>* mice following podocyte loss but not in *RenWt1<sup>fl/fl</sup>* mice.

### CoRL Migration to the Glomerulus Is Reduced in *RenWt1<sup>fl/fl</sup>* Mice Following Podocyte Depletion

Triple staining was performed for p57 (podocytes), RFP (TdTomato<sup>+</sup>, CoRL), and collagen IV (demarcates glomeruli) to determine if deleting WT1 reduced CoRL migration from the JGC to the glomerulus following abrupt podocyte loss. RFP<sup>+</sup>CoRL were rarely detected in glomeruli at baseline of either *RenWt1<sup>+/+</sup>* or *RenWt1<sup>fl/fl</sup>* mice (Figures 4A, 4D and 4G). At D28 FSGS in *RenWt1<sup>+/+</sup>* mice, RFP<sup>+</sup>CoRL were detected in  $3.5\% \pm 2.4\%$  of glomeruli compared with baseline ( $0.43\% \pm 0.2\%$ ;  $p = 0.013$ ; Figures 4B and 4G). At D28 FSGS in *RenWt1<sup>fl/fl</sup>* mice, RFP<sup>+</sup>CoRL were barely detected in glomeruli compared with *RenWt1<sup>+/+</sup>* mice ( $p = 0.001$ ; Figures 4E and 4G). Consistent with our recent report (Lichtnekert et al., 2016), administering enalapril to *RenWt1<sup>+/+</sup>* mice following podocyte depletion increased the migration of RFP<sup>+</sup>CoRL to  $12.95\% \pm 3.07\%$  of glomeruli compared with untreated ( $p < 0.001$ ; Figures 4C and 4G). However, enalapril had little impact on RFP<sup>+</sup>CoRL migration to glomeruli in *RenWt1<sup>fl/fl</sup>* mice (Figures 4F and 4G). Staining for renin and Cre was not detected in glomerular cells in disease, consistent with CoRL migration to the glomerulus rather than ectopic renin expression in disease. These results were similar to our previous reports (Pippin et al., 2013).

Figures S4 and 4C show that once RFP<sup>+</sup>CoRL migrated from the JGC to the glomerulus, a subset *de novo* co-express podocyte markers P57 (Figure 4C) podocin (Figure S4A–S4A4) and synaptopodin (Figure S4B–S4B4), consistent with CoRL transdifferentiating toward a podocyte fate.

These results show that WT1 is critical for CoRL migration to the glomerulus following podocyte loss and their transdifferentiation. In the absence of WT1, enalapril has reduced efficacy on CoRL migration and transdifferentiation.

### WT1 Is Important for CoRL Proliferation Following Podocyte Depletion

To test the role of WT1 in CoRL proliferation, bromodeoxyuridine (BrdU) was administered via intraperitoneal injections every 48 hr, starting at D2. Triple staining was performed for BrdU, WT1, and RFP to determine if proliferation was restricted to RFP<sup>+</sup>CoRL that co-expressed WT1,

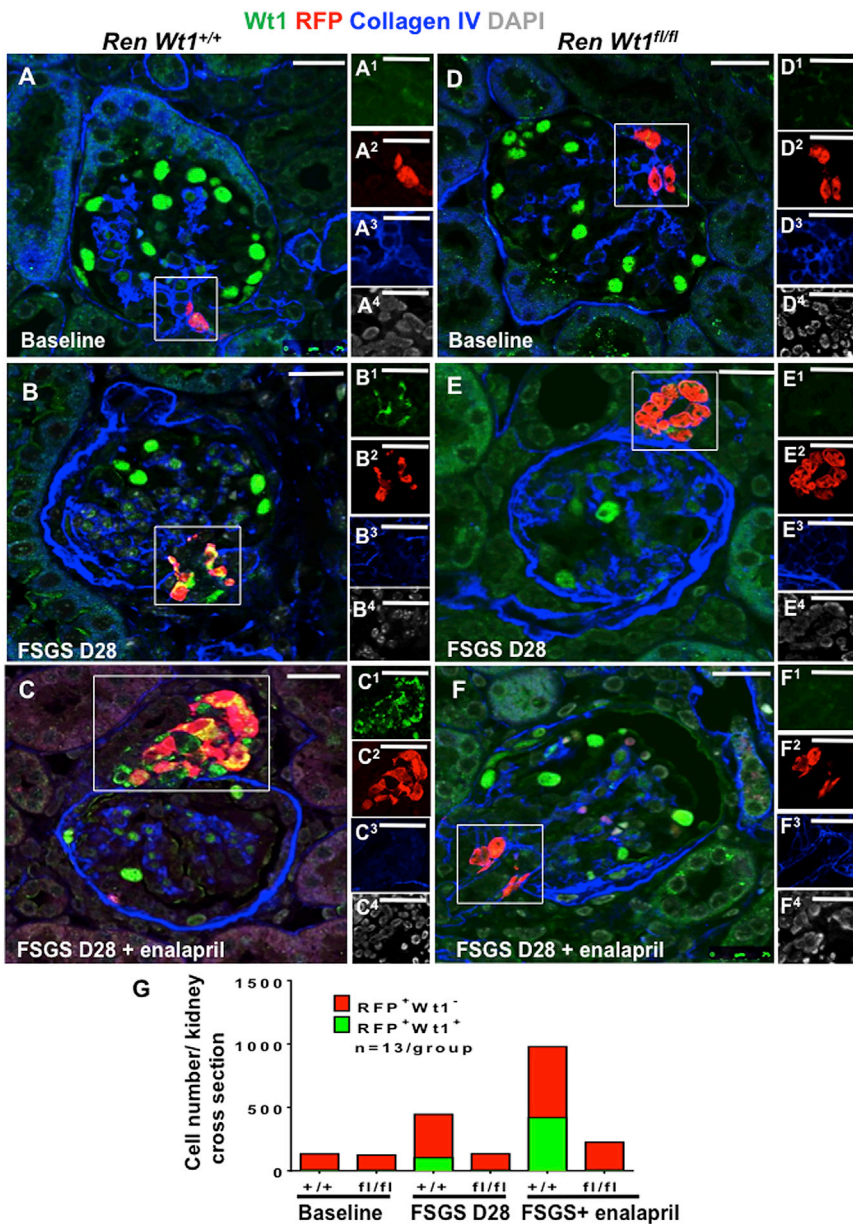


**Figure 3. WT1 Does Not Increase in CoRL in *RenWt1<sup>fl/fl</sup>* Mice Following Podocyte Depletion in the Cytotoxic Anti-podocyte Antibody Model of FSGS**

Confocal microscopy for WT1 (green), RFP (red), collagen IV (blue), and DAPI (gray) in FSGS in *RenWt1<sup>+/+</sup>* (A–C) and *RenWt1<sup>fl/fl</sup>* (D–F) mice. Insets show the JGC for each channel, labeled as superscripts. Scale bars, 20  $\mu$ m.

(A–C) *RenWt1<sup>+/+</sup>* mice. (A) At baseline WT1 is limited to podocytes (A1); RFP is limited to the JGC (A2). (B) At D28, WT1 (B1) merges with RFP (B2) in the JGC, creating a yellow color. WT1 is reduced in glomeruli. (C) At D28, after 25 days of enalapril, WT1 (C1) and RFP (C2) are increased in the JGC. (D–F) *RenWt1<sup>fl/fl</sup>* mice. (D) At baseline, WT1 (D1) is limited to podocytes; RFP (D2) is limited to JGC. (E) At D28, WT1 is reduced in podocytes, and not detected (E1) in RFP<sup>+</sup> cells (E2) in the JGC. (F) At D28, after 25 days of enalapril, there is no WT1(F1) in RFP<sup>+</sup> cells (F2).

(G) Stacked bar graph shows the number of RFP<sup>+</sup>CoRL not expressing WT<sup>-</sup> (red) and co-expressing WT<sup>+</sup> (green) in the JGC. RFP<sup>+</sup>WT<sup>+</sup> cells increase progressively in diseased *RenWt1<sup>+/+</sup>* but not in *RenWt1<sup>fl/fl</sup>* mice (n = 13/group).

and if WT1 is necessary for CoRL proliferation? BrdU was absent in RFP<sup>+</sup>CoRL at baseline in *RenWt1<sup>+/+</sup>* and *RenWt1<sup>fl/fl</sup>* mice (Figures 5A, 5D, and 5G). This was not a false negative, as BrdU was detected in neighboring tubules. Following podocyte depletion in *RenWt1<sup>+/+</sup>* mice, BrdU increased in RFP<sup>+</sup>WT1<sup>+</sup> cells compared with baseline (25.8  $\pm$  9.2 versus 0.8  $\pm$  0.5; p < 0.01; Figures 5B and 5G). In contrast, BrdU was barely detected in RFP<sup>+</sup>CoRLs in *RenWt1<sup>fl/fl</sup>* mice (Figures 5E and 5G). In enalapril-treated *RenWt1<sup>+/+</sup>* FSGS mice, RFP<sup>+</sup>WT1<sup>+</sup>BrdU<sup>+</sup> cells in the JGC increased compared with untreated mice (131.3  $\pm$  51.7 versus 25.8  $\pm$  9.2; p = 0.0001; Figures 5C and 5G). In enalapril-treated *RenWt1<sup>fl/fl</sup>* FSGS mice, RFP<sup>+</sup>WT1<sup>+</sup>BrdU<sup>+</sup> cells did

not increase (Figures 5F and 5G). To test WT1 independent proliferation, we counted RFP<sup>+</sup>BrdU<sup>+</sup>WT1<sup>-</sup> cells. BrdU was only observed in a small portion of RFP<sup>+</sup>WT1<sup>-</sup> cells in *RenWt1<sup>+/+</sup>* FSGS mice compared with baseline (5  $\pm$  0.8 versus 0.3  $\pm$  0.5; p < 0.05; Figures 5B, 5C, and 5G).

Triple staining was also performed for the proliferation marker Ki67, WT1, and RFP (Figure S7). Ki67 was not detected in RFP<sup>+</sup>CoRL at baseline in *RenWt1<sup>+/+</sup>* and *RenWt1<sup>fl/fl</sup>* mice (Figures S7A and S7D) but was detected in neighboring tubules. Following podocyte depletion, Ki67 increased in RFP<sup>+</sup> WT1<sup>+</sup>CoRL (Figure S7B), which was augmented by enalapril (Figure S7C). In *RenWt1<sup>fl/fl</sup>* mice, Ki67 was barely detected in RFP<sup>+</sup>CoRL (Figures S7E and S7F).

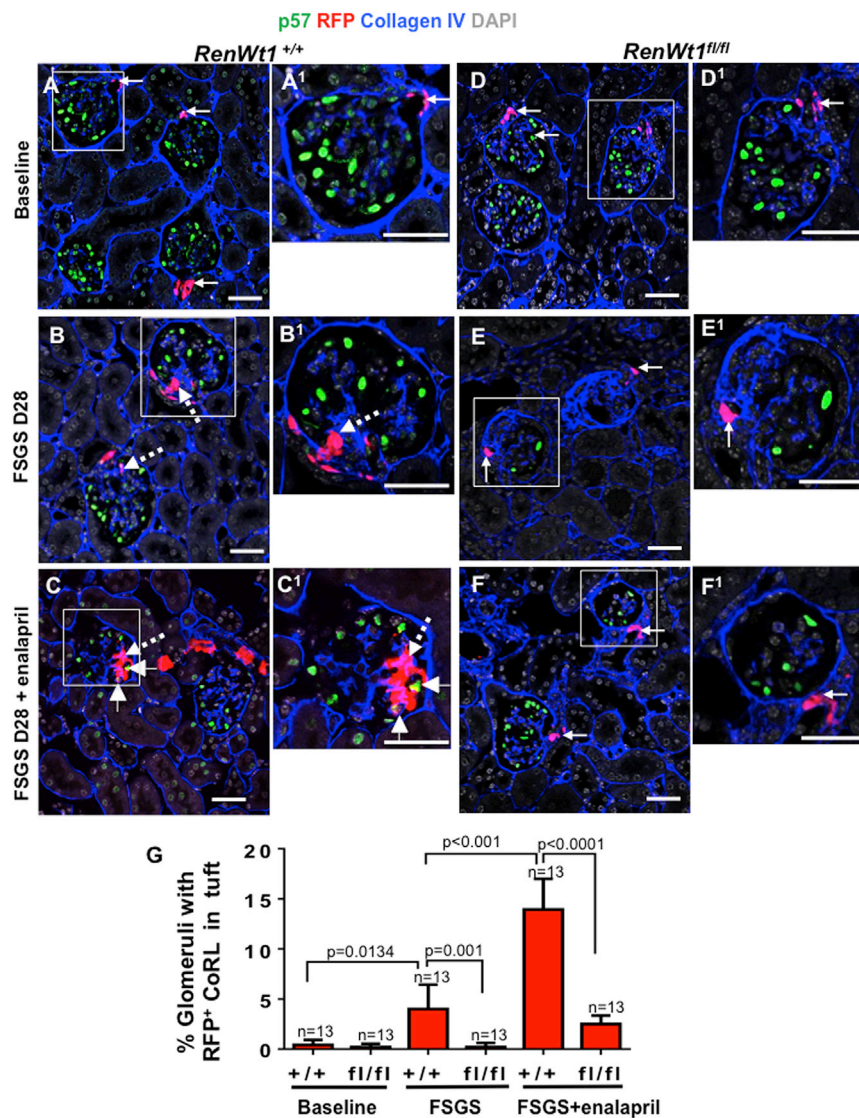


**Figure 4. RFP<sup>+</sup>CoRL Migration to the Glomerulus Is Significantly Reduced in Diseased *RenWt1<sup>fl/fl</sup>* Mice Compared with Diseased *RenWt1<sup>+/+</sup>* Mice**

Confocal microscopy for p57 (green, podocytes), RFP (red, CoRL), collagen IV (blue, demarcates glomerulus), and DAPI (gray, nucleus). Insets show the glomerulus marked with a white box, labeled as super-scripts. Scale bars, 20  $\mu$ m.

(A–C) *RenWt1<sup>+/+</sup>* mice. (A, A1) In baseline *RenWt1<sup>+/+</sup>* mice, RFP<sup>+</sup>CoRL (solid arrows) are restricted to the JGC and p57 to podocytes. (B, B1) A serial biopsy at D28 in the same *RenWt1<sup>+/+</sup>* mouse from (A). RFP<sup>+</sup>CoRL are in glomeruli (dashed arrows). (C, C1) At FSGS D28 after enalapril, RFP<sup>+</sup>CoRL in both the JGC and glomeruli are further increased and a subset in the tuft *de novo* express the podocyte marker p57 (arrowheads).

(D–F) *RenWt1<sup>fl/fl</sup>* mice. (D, D1) In baseline *RenWt1<sup>fl/fl</sup>* mice, RFP<sup>+</sup>CoRL (solid arrows) are restricted to the JGC and p57 to podocytes. (E, E1) At D28, despite the decrease in p57 (podocytes), RFP<sup>+</sup>CoRL remain restricted to the JGC (arrow). (F, F1) At D28 after enalapril, RFP<sup>+</sup>CoRL were mostly limited to the JGC.

(G) Quantitation of the percentage of glomeruli with RFP<sup>+</sup>CoRL increased progressively in diseased *RenWt1<sup>+/+</sup>* mice but not in diseased *RenWt1<sup>fl/fl</sup>* mice (n = 13/group).

These results show that after podocyte depletion, the following occurs: (1) proliferation (BrdU<sup>+</sup> or Ki67<sup>+</sup>) of CoRL (RFP<sup>+</sup>) occurs in cells co-expressing WT1; (2) CoRL proliferation was reduced in *RenWt1<sup>fl/fl</sup>* mice; (3) enalapril increased CoRL proliferation in diseased *RenWt1<sup>+/+</sup>* but not in *RenWt1<sup>fl/fl</sup>* mice.

#### Following Podocyte Loss, CoRL that Migrate to the Glomerulus Lose Mesenchymal Markers and *De Novo* Acquire Epithelial Markers

CoRL and podocytes derive from mesenchymal lineages (Boyle et al., 2008; Kobayashi et al., 2008; Costantini and Kopan, 2010; Little and McMahon, 2012). To determine if WT1 in CoRL is necessary for changes in mesenchymal and epithelial cell markers, and if these changes were augmented by enalapril, additional studies were per-

formed (Figures 6 and S6). Staining for the mesenchymal marker myosin heavy chain 11 (MYH11) was detected in 90%  $\pm$  7.5% and 84.1%  $\pm$  8.2% of RFP<sup>+</sup>CoRL in the JGC in baseline *RenWt1<sup>+/+</sup>* and *RenWt1<sup>fl/fl</sup>* mice, respectively (Figures 6A, 6D, and 6G). Following podocyte depletion in *RenWt1<sup>+/+</sup>* mice, the percentage of MYH11<sup>+</sup>RFP<sup>+</sup> cells decreased to 67.5%  $\pm$  5.3% compared with baseline (p = 0.0059; Figures 6B and 6G). The percentage of MYH11<sup>+</sup>RFP<sup>+</sup> cells did not decrease in *RenWt1<sup>fl/fl</sup>* mice with FSGS compared with baseline (82.6%  $\pm$  10.6% versus 84.1%  $\pm$  8.2%; p = 0.99; Figures 6E and 6G). In enalapril-treated FSGS *RenWt1<sup>+/+</sup>* mice, MYH11<sup>+</sup>RFP<sup>+</sup>CoRL decreased (44.3% versus 67.5%; p = 0.008; Figures 6C and 6G). Giving enalapril to *RenWt1<sup>fl/fl</sup>* mice did not reduce MYH11<sup>+</sup>RFP<sup>+</sup>CoRL (78.7% versus 82.6%; p > 0.99; Figures 6F and 6G). CoRL that migrated to

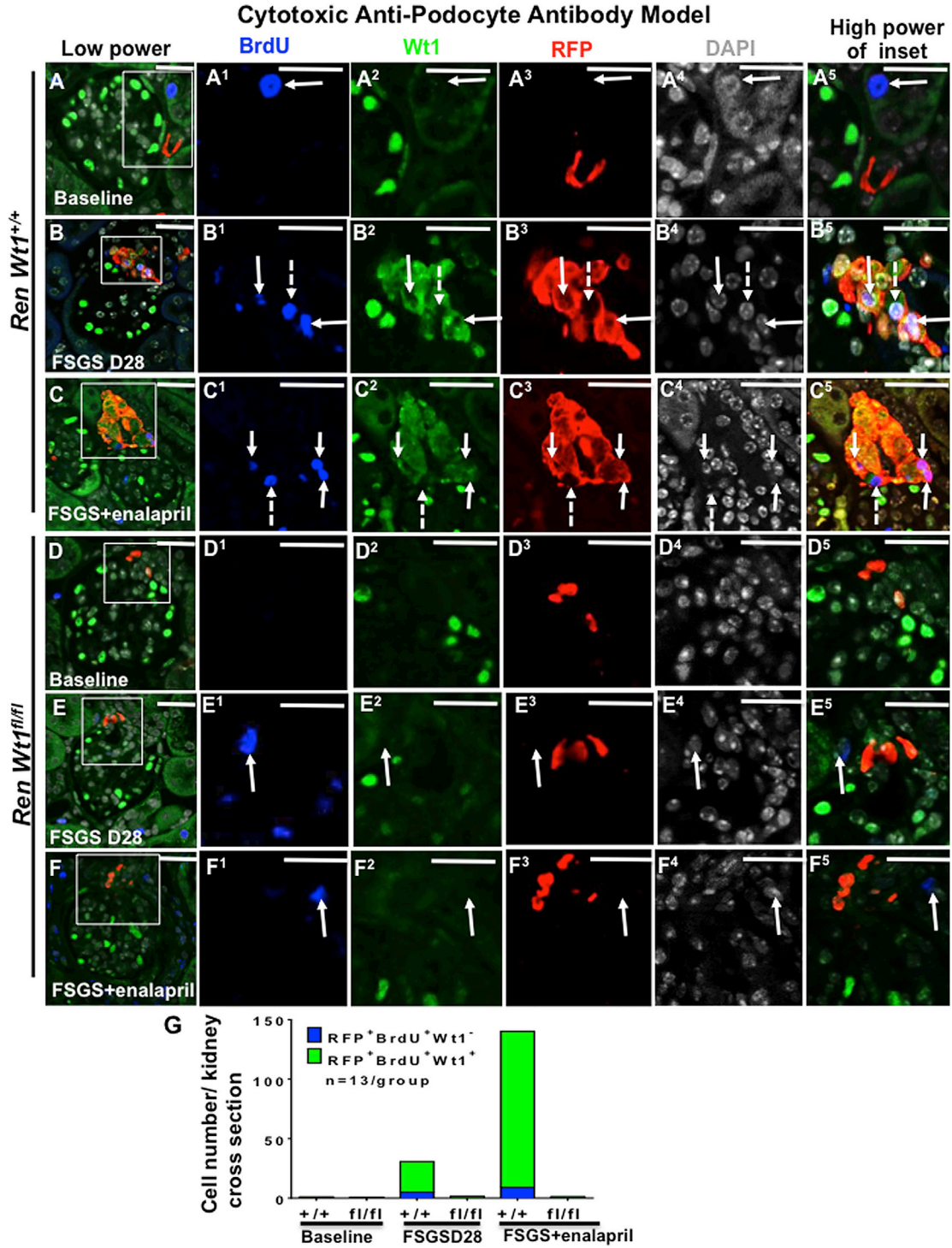


**Figure 5. RFP\*CoRL Proliferation Is Significantly Reduced in Diseased *RenWt1<sup>fl/fl</sup>* Mice Compared with Diseased *RenWt1<sup>+/+</sup>* Mice**  
 Confocal microscopy for BrdU (blue), WT1 (green), RFP (red), and DAPI (gray) in experimental FSGS in *RenWt1<sup>+/+</sup>* and *RenWt1<sup>fl/fl</sup>* mice. Insets show the JGC for each channel, labeled as superscripts. Scale bars, 20  $\mu$ m.

(A–C) *RenWt1<sup>+/+</sup>* mice. (A) At baseline, a BrdU<sup>+</sup> cell (A1) is detected in the adjacent tubule. BrdU is not detected in the JGC. WT1 (A2) is not detected in RFP<sup>+</sup> cells (A3). (B) At FSGS D28, BrdU (B1) co-localizes with WT1 (B2) and RFP (B3), creating a white/purple color (B5, solid

(legend continued on next page)



glomeruli did not stain for MYH11 with either strain (data not shown).

In RFP<sup>+</sup>CoRL in the JGC, the epithelial cell marker cytokeratin 18 (CK18) was barely detected at baseline in either *RenWt1*<sup>+/+</sup> or *RenWt1*<sup>fl/fl</sup> mice (Figures 6H, 6K, and 6N). At D28 FSGS in *RenWt1*<sup>+/+</sup> mice, the percentage of RFP<sup>+</sup>CK18<sup>+</sup>CoRL in the JGC increased compared with baseline (16.8% ± 2.4% versus 1.5% ± 0.9%; *p* < 0.0001; Figures 6I and 6N). The percentage of RFP<sup>+</sup>CK18<sup>+</sup>CoRL was further increased by enalapril compared with baseline (27.25% ± 6.08% versus 16.75% ± 2.36%; *p* < 0.0001; Figures 6J and 6N). In contrast, in *RenWt1*<sup>fl/fl</sup> mice, the percentage of RFP<sup>+</sup>CK18<sup>+</sup>CoRL did not increase (2.8% ± 3.5% versus 1.5% ± 0.8%; *p* = 0.606; Figures 6K, 6L, and 6N), and enalapril had no impact (3.7% ± 3.1% versus 2.8% ± 3.5% versus FSGS without enalapril; *p* > 0.99) (Figures 6K, 6M, and 6N).

Figure S6 confirms these results using additional mesenchymal and epithelial cell markers. The mesenchymal markers  $\alpha$ SMA (Figures S6A–S6F) and smooth muscle protein 22 (SM22) (Figures S6G–S6L) were abundant in RFP<sup>+</sup>CoRL in the JGC at baseline in both strains (Figures S6A, S6D, S6G, and S6J). Co-staining for both mesenchymal markers decreased in *RenWt1*<sup>+/+</sup> mice with FSGS (Figures S6B and S6H), and was further decreased by enalapril (Figures S6C and S6I). No RFP<sup>+</sup>CoRL in glomeruli co-expressed  $\alpha$ SMA or SM22 (Figures 6A and 6C). In contrast,  $\alpha$ SMA<sup>+</sup>/RFP<sup>+</sup>CoRL and SM22<sup>+</sup>/RFP<sup>+</sup>CoRL did not decrease in *RenWt1*<sup>fl/fl</sup> mice with FSGS, or with enalapril (Figures S6E, S6F, S6K, and S6L).

The epithelial cell marker E-cadherin was not detected in RFP<sup>+</sup> cells in the JGC at baseline in either *RenWt1*<sup>+/+</sup> or *RenWt1*<sup>fl/fl</sup> mice (Figures S6M and S6P). Following podocyte depletion in *RenWt1*<sup>+/+</sup> mice, RFP<sup>+</sup> cells in the JGC *de novo* expressed E-cadherin, which was augmented by enalapril (Figures S6N and S6O). In contrast, E-cadherin staining was not detected in the JGC in *RenWt1*<sup>fl/fl</sup> mice following podocyte depletion, and enalapril had no effect (Figures S6Q and S6R).

Following podocyte depletion in *RenWt1*<sup>+/+</sup> mice, a subset of CoRL that migrated from the JGC (Figures S5A1–S5A4, S5B1–S5B4, and S5C1–S5C4) to the glomerular tuft no longer expressed  $\alpha$ SMA (Figure S5A5–S5A8). There was *de novo* expression in CoRL in glomeruli of the epithelial markers E-cadherin (Figure S5B5–S5B8) and cytokeratin

18 (Figure S5C5–S5C8), coincident with loss of mesenchymal markers.

These results show that following abrupt podocyte depletion, mesenchymal markers (MYH11,  $\alpha$ SMA, SM22) decrease in CoRL, coincident with *de novo* staining for the epithelial cell markers cytokeratin 18 and E-cadherin (Figure S6S). These events were augmented by enalapril in *RenWt1*<sup>+/+</sup> mice, supporting the notion that CoRL undergo MET in *RenWt1*<sup>+/+</sup> mice with FSGS, but these events are significantly reduced when WT1 is deleted.

### Podocyte Replacement Is Lower in Diseased *RenWt1*<sup>fl/fl</sup> Mice

The binding of the podocyte-depleting antibody was similar in *RenWt1*<sup>+/+</sup> and *RenWt1*<sup>fl/fl</sup> mice (Figures S2J and S2K). Podocyte density, measured by quantitating p57, was similar at baseline in *RenWt1*<sup>+/+</sup> and *RenWt1*<sup>fl/fl</sup> mice (Figures 7A, 7B, and 7E). Podocyte density decreased in *RenWt1*<sup>+/+</sup> mice with FSGS compared with baseline (185.2 ± 17.1 × 10<sup>6</sup> versus 250.7 ± 10.0 × 10<sup>6</sup> podocytes/ $\mu$ m<sup>3</sup> glomerular tuft volume; *p* < 0.0001; Figures 7C and 7E). Moreover, podocyte density was significantly lower in diseased *RenWt1*<sup>fl/fl</sup> mice compared with diseased *RenWt1*<sup>+/+</sup> mice (109.3 ± 10.09 × 10<sup>6</sup> versus 185.2 ± 17.1 × 10<sup>6</sup> podocytes/ $\mu$ m<sup>3</sup>; *p* < 0.001; Figures 7D and 7E). Similar findings were shown for podocin (Figures 7G–7J). Glomerulosclerosis increased in diseased *RenWt1*<sup>+/+</sup> mice but was significantly higher in diseased *RenWt1*<sup>fl/fl</sup> mice (Figure 7F). The urinary albumin to creatinine ratio was also significantly higher in diseased *RenWt1*<sup>fl/fl</sup> mice (Figure 7K). In summary, podocyte density was lower in *RenWt1*<sup>fl/fl</sup> mice compared with *RenWt1*<sup>+/+</sup> mice, accompanied by higher glomerulosclerosis and albuminuria.

## DISCUSSION

Adult podocytes cannot proliferate and are unable to self-renew following depletion (Barisoni et al., 2000; Pavenstadt et al., 2003). Their replacement in glomerular diseases is reliant on progenitors (Romagnani et al., 2013; Shankland et al., 2014). CoRL plasticity has been reported in podocytes, PECs, kidney pericytes, and mesangial cells (Gomez et al., 2014; Pippin et al., 2015; Starke et al., 2015; Kaverina et al., 2016; Stefanska et al., 2016). To serve

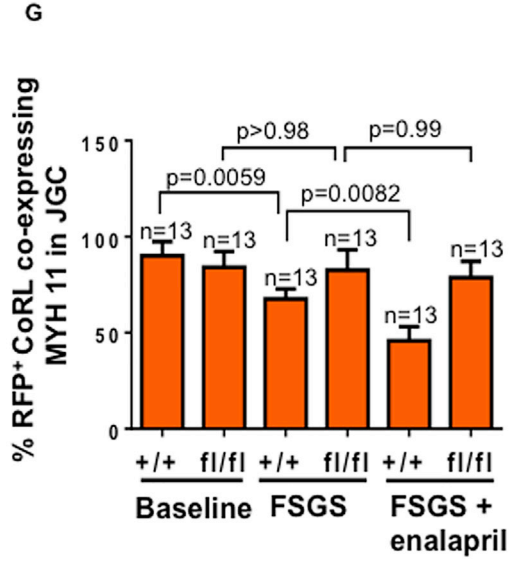
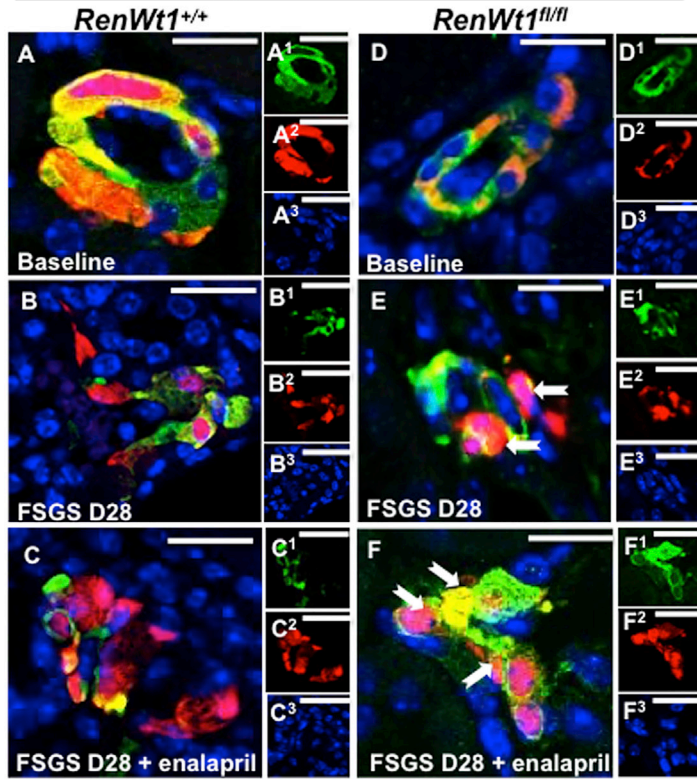
arrows). A few BrdU<sup>+</sup> cells do not express WT1 (B1–B5, dashed arrow) (C) At D28 after enalapril, BrdU<sup>+</sup> (C1), WT1<sup>+</sup> (C2), RFP<sup>+</sup> (C3) cells increase (C5, solid arrows). A few BrdU<sup>+</sup> cells do not express WT1 (C1–C5, dashed arrow).

(D–F) *RenWt1*<sup>fl/fl</sup> mice. (D) At baseline, neither BrdU (D1) nor WT1 (D2) is detected in RFP<sup>+</sup> (D3) cells in the JGC. (E) At D28, a BrdU<sup>+</sup> cell (E1, solid arrow) is detected in the adjacent tubule and does not overlap with WT1 (E2) or RFP (E3), hence no merge (E5). (F) At D28 after enalapril, a BrdU<sup>+</sup> cell (F1, solid arrow) does not overlap with WT1 (F2) or RFP (F3), hence no merge (F5).

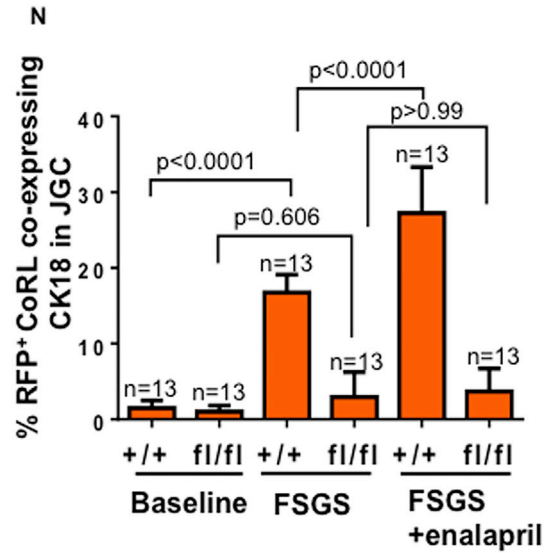
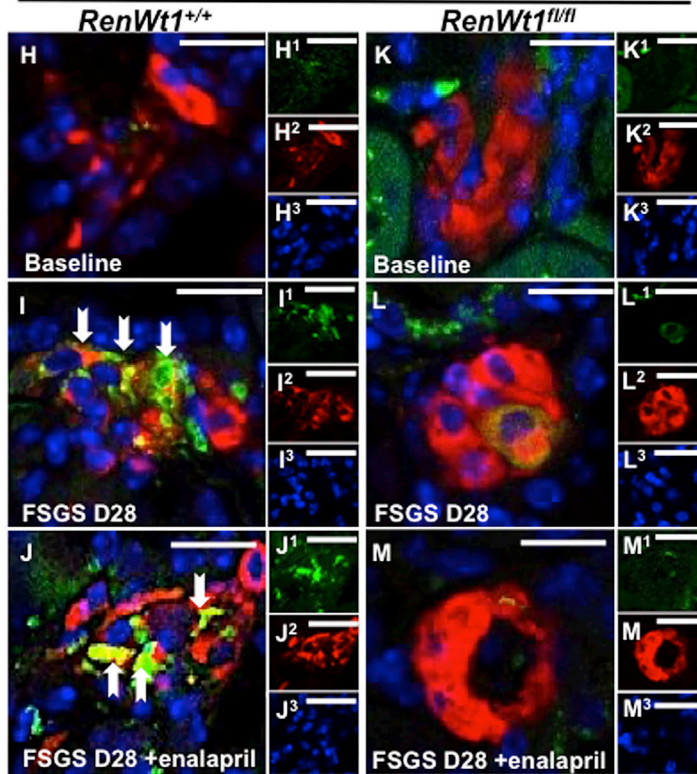
(G) Stacked bar graph shows the number of RFP<sup>+</sup>BrdU<sup>+</sup>WT1<sup>-</sup> (blue) and RFP<sup>+</sup>BrdU<sup>+</sup>WT1<sup>+</sup> (green) cells in the JGC. RFP<sup>+</sup>BrdU<sup>+</sup>WT1<sup>+</sup> cells increase progressively in diseased *RenWt1*<sup>+/+</sup> mice but not in *RenWt1*<sup>fl/fl</sup> mice (*n* = 13/group).



Myosin11 RFP DAPI



Cytokeratin18 RFP DAPI



(legend on next page)



as progenitors for podocytes, CoRL must increase in number, migrate from the JGC to the glomerulus, and reprogram from a mesenchymal to an epithelial fate. To better understand the mechanisms underlying these events, we selectively genetically deleted WT1 in CoRL in transgenic mice. Reducing podocytes with a cytopathic anti-podocyte antibody resulted in a significant reduction in CoRL proliferation, migration, and MET, suggesting a critical role for WT1.

We show that WT1 staining is detected in <5%–7% of renin-expressing cells in the JGC in normal mice and rats, and only occasionally in the JGC in normal human kidneys, similar to previous reports (Puelles et al., 2015). The first major result of the studies was that following podocyte depletion in three experimental models, WT1 increased up to 5.5-fold from baseline in renin-expressing cells in the JGC. WT1 also increased in renin-expressing cells in human FSGS and membranous nephropathy. WT1 did not increase following uninephrectomy, serving as a negative control because podocyte number was unchanged.

The role for WT1 is well described in podocyte health (Ozdemir and Hohenstein, 2014; Mazzei and Manucha, 2016), in non-kidney cell transdifferentiation (Ijpenberg et al., 2007), and progenitor function (Martinez-Estrada et al., 2010; Bandiera et al., 2013). To test the hypothesis that WT1 is necessary for CoRL to function as podocyte progenitors, we generated a transgenic mouse where WT1 was inducibly deleted specifically in CoRL. Under non-stressed conditions, deleting WT1 in CoRL had no impact on kidney or podocyte function and morphology.

CoRL migrate from the JGC to the glomerulus or tubulointerstitium during kidney development and in disease (Sequeira Lopez et al., 2004; Pippin et al., 2013, 2015; Starke et al., 2015; Zhang et al., 2015; Lichtnekert et al., 2016). Here, RFP<sup>+</sup>CoRL were rarely detected in glomeruli

of non-diseased *RenWt1*<sup>+/+</sup> and *RenWt1*<sup>fl/fl</sup> mice. However, RFP<sup>+</sup>CoRL were readily detected in glomeruli in *RenWt1*<sup>+/+</sup> mice following podocyte depletion, similar to previous reports (Pippin et al., 2013; Lichtnekert et al., 2016). The second major finding was that following podocyte depletion, RFP<sup>+</sup>CoRL were barely detected in glomeruli of *RenWt1*<sup>fl/fl</sup> mice, and migration to the glomerulus was not augmented by enalapril in *RenWt1*<sup>fl/fl</sup> mice. These results are consistent with WT1 being necessary for CoRL migration and the enhanced migratory effects of enalapril. Similar results in the cancer field suggest that WT1 enhances cell invasion and migration (Jomgeow et al., 2006; Brett et al., 2013).

CoRL increase in the JGC following podocyte depletion (Pippin et al., 2013, 2014), increased glomerular volume (Hodgin et al., 2015), hypotension (Castellanos Rivera et al., 2011), and following angiotensin-converting enzyme (ACE) inhibitors and angiotensin receptor blockers (Lichtnekert et al., 2016). BrdU and Ki67 staining showed that following podocyte depletion in *RenWt1*<sup>+/+</sup> mice, RFP<sup>+</sup>CoRL proliferated, which was augmented by enalapril (Duim et al., 2015; Lichtnekert et al., 2016). A third major finding was no increase in CoRL proliferation in *RenWt1*<sup>fl/fl</sup> mice, and enalapril had no effect. This was of interest, as several groups have shown that WT1 enhances proliferation of tumor cells and cardiac endothelial cells (Li et al., 2015; Wu et al., 2015).

Like podocytes (Boyle et al., 2008; Kobayashi et al., 2008), CoRL derive from mesenchymal origins (Sequeira Lopez et al., 2001; Matsushita et al., 2010; Wang et al., 2013; Ciampi et al., 2016). To become podocytes, CoRL need to decrease mesenchymal proteins and acquire epithelial and podocyte proteins. At baseline, RFP<sup>+</sup>CoRL in the JGC in both *RenWt1*<sup>+/+</sup> and *RenWt1*<sup>fl/fl</sup> mice express mesenchymal markers (MYH11,  $\alpha$ SMA, SM22) but not

### Figure 6. RFP<sup>+</sup>CoRL MET Is Significantly Reduced in Diseased *RenWt1*<sup>fl/fl</sup> Mice Compared with Diseased *RenWt1*<sup>+/+</sup> Mice

Confocal microscopy for myosin11 (MYH11, green, mesenchymal marker), RFP (red, CoRL), and DAPI (blue, nuclei) in the JGC (A–F). Insets show each channel, labeled as superscripts. Scale bars, 20  $\mu$ m.

(A–C) *RenWt1*<sup>+/+</sup> mice. (A) At baseline, MYH11 (A1) merges with RFP (A2) in the JGC, creating a yellow color. (B) At FSGS D28, MYH11 (B1) decreases in RFP<sup>+</sup> (B2) cells. (C) At D28 after enalapril, MYH11 (C1) decreases, despite an increase in RFP<sup>+</sup> cells (C2).

(D–F) *RenWt1*<sup>fl/fl</sup> mice. (D) At baseline, MYH11 (D1) merges with RFP (D2). (E) At FSGS D28, MYH11 (E1) in RFP<sup>+</sup> cells (E2, solid arrows) persists. (F) At D28 after enalapril, MYH11 (F1) in RFP<sup>+</sup> cells (F2, solid arrows) also persists.

(G) The percentage of RFP<sup>+</sup>CoRL expressing MYH11 decreases in *RenWt1*<sup>+/+</sup> mice with FSGS and is augmented by enalapril. *RenWt1*<sup>fl/fl</sup> mice show no significant decrease in MYH11 (n = 13/group).

(H–M) Confocal microscopy for cytokeratin 18 (CK18, green, epithelial marker), RFP (red, CoRL), and DAPI (blue, nuclei) in the JGC (H–M). Insets show each channel, labeled as superscripts. Scale bars, 20  $\mu$ m.

(H–J) *RenWt1*<sup>+/+</sup> mice. (H) At baseline, CK18 (H1) is barely detected in RFP<sup>+</sup> cells (H2). (I) At FSGS D28, CK18 (I1) increases in RFP<sup>+</sup> cells (I2), creating a yellow color (solid arrows). (J) At D28 after enalapril, CK18 (J1) further increases in RFP<sup>+</sup> cells (J2), creating a yellow color (solid arrows).

(K–M) *RenWt1*<sup>fl/fl</sup> mice. (K) At baseline, CK18 (K1) is not detected in RFP<sup>+</sup> cells (K2). At FSGS D28 (L) and after enalapril (M), CK18 (L1, M1) does not increase in RFP<sup>+</sup> cells (L2, M2).

(N) The percentage of RFP<sup>+</sup>CK18<sup>+</sup> cells increases in diseased *RenWt1*<sup>+/+</sup> mice, which is augmented by enalapril. CK18 does not increase significantly in diseased *RenWt1*<sup>fl/fl</sup> mice (n = 13/group).

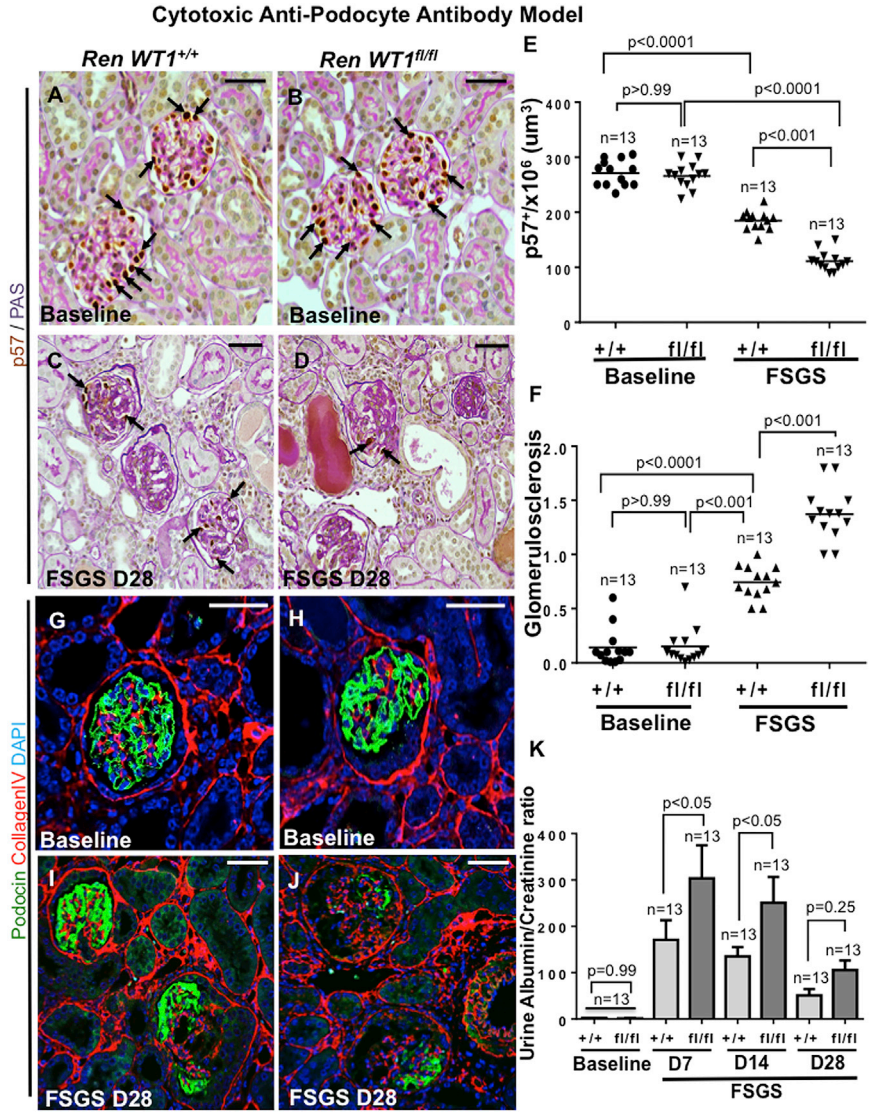


**Figure 7. Podocyte Depletion in the Cytotoxic Anti-podocyte Antibody Model of FSGS Is Higher in Diseased *RenWt1<sup>fl/fl</sup>* Mice than in Diseased *RenWt1<sup>+/+</sup>* Mice**

(A–F) Podocytes are identified by p57 (brown, nuclear, arrows) and matrix (pink) in a baseline biopsy from *RenWt1<sup>+/+</sup>* (A) and *RenWt1<sup>fl/fl</sup>* (B) mice, and a serial biopsy in the same mice at FSGS D28 (C and D). (E) Podocyte density was similar at baseline but lower in diseased *RenWt1<sup>fl/fl</sup>* compared with diseased *RenWt1<sup>+/+</sup>* mice. (F) Glomerulosclerosis is higher in diseased *RenWt1<sup>fl/fl</sup>* compared with diseased *RenWt1<sup>+/+</sup>* mice. (G–J) Podocin staining (green) is similar in healthy podocytes in baseline *RenWt1<sup>+/+</sup>* (G) and *RenWt1<sup>fl/fl</sup>* (H) mice. Podocin decreases at FSGS D28 in *RenWt1<sup>+/+</sup>* mice (I) and is more pronounced in diseased *RenWt1<sup>fl/fl</sup>* mice (J). Scale bars, 20 μm. (K) Urinary albumin to creatinine ratio in *RenWt1<sup>fl/fl</sup>* mice (dark bars) is higher than *RenWt1<sup>+/+</sup>* mice (light bars) (n = 13/group).

epithelial markers (cytokeratin 18, E-cadherin). Following podocyte depletion in *RenWt1<sup>+/+</sup>* mice, RFP<sup>+</sup>CoRL in the JGC expressing these mesenchymal markers decreased significantly. This coincided with the *de novo* expression of cytokeratin 18 and E-cadherin. The MET-like changes in diseased *RenWt1<sup>+/+</sup>* mice were augmented by enalapril. When in the glomerulus, a subset of CoRL co-expressed the podocyte markers p57, podocin, and synaptopodin. The fourth major finding was that following podocyte depletion in *RenWt1<sup>fl/fl</sup>* mice, mesenchymal markers in RFP<sup>+</sup> CoRL did not decrease, nor did they begin to express epithelial markers, and enalapril had no impact.

These findings are consistent with our previous reports on the importance of disruption of MET underlying the origin of Wilms' tumors (Berry et al., 2015; Hohenstein et al., 2015), the role of *Wt1* in this MET programming (Da-

vies et al., 2004; Essafi et al., 2011), and that loss of WT1 blocks MET in the cap mesenchyme (Essafi et al., 2011).

The fifth major finding was that following abrupt podocyte loss, podocyte density remained lower in diseased *RenWt1<sup>fl/fl</sup>* compared with diseased *RenWt1<sup>+/+</sup>* mice, accompanied by more glomerular scarring and albuminuria. We recognize that CoRL transdifferentiation alone is not sufficient to explain the differences, and other factors including different kidney progenitor populations need to be considered.

Finally, our observation of intra-glomerular CoRL with coincident downregulation of renin expression would be consistent with the negative regulation previously described (Steege et al., 2008). It will be of interest to assess the specific isoform(s) of WT1 expressed and retained in CoRL and the kinetics of renin downregulation and other



cell differentiation features altered as a function of this interaction.

In summary, WT1 expression in CoRL is important for the glomerular response to damage. When WT1 is selectively deleted in CoRL in the setting of podocyte loss, their proliferation and migration to the glomerulus, and to some extent their transdifferentiation toward a podocyte fate through MET changes, are markedly reduced.

## EXPERIMENTAL PROCEDURES

### *RenCreER tdTomato Wt1<sup>+/+</sup>* and *Wt1<sup>fl/fl</sup>* Reporter Mice

*Ren1cCreERxRs-tdTomato-R* mice (Pippin et al., 2013) were crossed with a *Wt1* conditional knockout mouse (*Wt1<sup>fl/fl</sup>*) (Martinez-Estrada et al., 2010). *Wt1* was inactivated in *RenCreER tdTomato Wt1<sup>fl/fl</sup>* mice (abbreviated *RenWt1<sup>fl/fl</sup>*) by administration of 100 mg/kg tamoxifen on four occasions. Mouse genotype was identified by PCR (Martinez-Estrada et al., 2010). Kidney biopsies were performed to assess CoRL labeling as described in Supplemental Experimental Procedures. *RenWt1<sup>fl/fl</sup>* and *RenWt1<sup>+/+</sup>* were housed in the animal care facility of the University of Washington (UW) under specific pathogen-free conditions with food and water available ad libitum. These studies were reviewed and approved by the UW Institutional Animal Care and Use Committee (2968-04).

### Experimental Models of Glomerular Disease Accompanied by Podocyte Depletion

The following experimental models of podocyte depletion were used:

- (1) A cytotoxic sheep anti-glomerular antibody model of experimental FSGS was induced in *RenWt1<sup>fl/fl</sup>* and *RenWt1<sup>+/+</sup>* mice as previously described (Kaverina et al., 2016; Lichtnekert et al., 2016). On D3, when podocyte number was decreased by 30%–40%, mice were randomized into two groups: group 1 received drinking water; group 2 received the ACE inhibitor enalapril (75 mg/mL). Mice were killed on D28. Urine was collected at baseline, and on days 7, 14, and 28. Amersham Cell Proliferation Labeling Reagent (GE Healthcare Life Sciences, Little Chalfont, UK) was administered to quantitate cell proliferation (Kaverina et al., 2016). Urines were collected for albumin measurements by radial immunodiffusion assay (RID) (Marshall et al., 2011); urine creatinine was measured by colorimetric micro-plate assay (Cayman Chemical Company, Ann Arbor, MI).
- (2) Podocyte TGF $\beta$ -Receptor1 transgenic (*PodTgfb1*) mice given doxycycline underwent TGF $\beta$ R1-induced podocyte apoptosis and loss of 25% (D7) and 40% (D14), accompanied by glomerulosclerosis (Daehn et al., 2014).
- (3) A PHN model of membranous nephropathy induced as previously described (Ohse et al., 2010) underwent progressive podocyte depletion (Petermann et al., 2003).
- (4) A uninephrectomy model served as a negative control for podocyte depletion (Pippin et al., 2015).

### Human Glomerular Disease

Kidney biopsies from patients with FSGS and membranous nephropathy were obtained from the University of Chicago (UC). The study protocol was approved by the UC Institutional Review Board. Further details are described in Supplemental Experimental Procedures.

### Laser Capture Microscopy and qRT-PCR

RFP<sup>+</sup>CoRL were isolated by LCM, as described (Tretiakova and Hart, 2011), with the Leica Laser Microdissection Systems LMD6500 and LMD7000 (Leica Microsystems Inc., Buffalo Grove, IL).

### Immunoperoxidase and Immunofluorescent Staining

Formalin-fixed paraffin-embedded mouse, rat, and human kidney sections or frozen tissue sections (4–20  $\mu$ m thick) were used. Following standard antigen retrieval steps, Avidin-biotin based, polymer-based, and fluorochrome-based staining was performed as previously described (Kimura et al., 1995; Wagner et al., 2014). Further details are described in Supplemental Experimental Procedures.

### Quantitative Analysis

Absolute numbers of renin<sup>+</sup>, RFP<sup>+</sup>, WT1<sup>+</sup>, and RFP<sup>+</sup>/WT1<sup>+</sup> expressing cells were counted in the JGC of fluorescence-stained sections. Results were expressed as a percentage of co-localized RFP<sup>+</sup>/WT1<sup>+</sup> cells per number of renin<sup>+</sup> cells. The percentage of proliferating (BrdU<sup>+</sup>) CoRL co-expressing WT1 in the JGC was measured by dividing the number of RFP<sup>+</sup>/WT1<sup>+</sup>/BrdU<sup>+</sup>-stained cells by the total number of RFP<sup>+</sup> cells in the JGC. The total number of glomeruli and glomeruli with RFP<sup>+</sup> cells were counted to determine the percentage of glomeruli with RFP<sup>+</sup> cells. Absolute numbers of RFP<sup>+</sup>, MYH11<sup>+</sup>, CK18<sup>+</sup>, MYH11<sup>+</sup>/RFP<sup>+</sup>, and CK18<sup>+</sup>/RFP<sup>+</sup>-expressing cells were counted in the JGC. Results were expressed as a percentage of MYH11<sup>+</sup>/RFP<sup>+</sup> and CK18<sup>+</sup>/RFP<sup>+</sup> cells per number of RFP<sup>+</sup> cells in the JGC. Podocyte number was measured on 150  $\pm$  20 glomeruli per animal on p57/periodic acid-Schiff-stained sections (Zhang et al., 2015; Lichtnekert et al., 2016).

### Statistical Analysis

Groups were compared using a one-way or two-way ANOVA for multiple comparisons with Bonferroni post hoc analysis with significant set at  $p < 0.05$ . Data are presented as means  $\pm$  SEM. All data were analyzed in GraphPad Prism 5.0 (GraphPad Software, La Jolla, CA).

## SUPPLEMENTAL INFORMATION

Supplemental Information includes Supplemental Experimental Procedures and seven figures and can be found with this article online at <http://dx.doi.org/10.1016/j.stemcr.2017.08.020>.

Received: January 20, 2017

Revised: August 25, 2017

Accepted: August 28, 2017

Published: September 28, 2017



## REFERENCES

- Bandiera, R., Vidal, V.P., Motamedi, F.J., Clarkson, M., Sahut-Barnola, I., von Gise, A., Pu, W.T., Hohenstein, P., Martinez, A., and Schedl, A. (2013). WT1 maintains adrenal-gonadal primordium identity and marks a population of AGP-like progenitors within the adrenal gland. *Dev. Cell* 27, 5–18.
- Barisoni, L., Mokrzycki, M., Sablay, L., Nagata, M., Yamase, H., and Mundel, P. (2000). Podocyte cell cycle regulation and proliferation in collapsing glomerulopathies. *Kidney Int.* 58, 137–143.
- Berry, R.L., Ozdemir, D.D., Aronow, B., Lindstrom, N.O., Dudnakova, T., Thornburn, A., Perry, P., Baldock, R., Armit, C., Joshi, A., et al. (2015). Deducing the stage of origin of Wilms' tumours from a developmental series of Wt1-mutant mice. *Dis. Model. Mech.* 8, 903–917.
- Boyle, S., Misfeldt, A., Chandler, K.J., Deal, K.K., Southard-Smith, E.M., Mortlock, D.P., Baldwin, H.S., and de Caestecker, M. (2008). Fate mapping using Cited1-CreERT2 mice demonstrates that the cap mesenchyme contains self-renewing progenitor cells and gives rise exclusively to nephronic epithelia. *Dev. Biol.* 313, 234–245.
- Brett, A., Pandey, S., and Fraizer, G. (2013). The Wilms' tumor gene (WT1) regulates E-cadherin expression and migration of prostate cancer cells. *Mol. Cancer* 12, 1–28.
- Castellanos Rivera, R.M., Monteagudo, M.C., Pentz, E.S., Glenn, S.T., Gross, K.W., Carretero, O., Sequeira-Lopez, M.L., and Gomez, R.A. (2011). Transcriptional regulator RBP-J regulates the number and plasticity of renin cells. *Physiol. Genomics* 43, 1021–1028.
- Chau, Y.Y., Brownstein, D., Mjoseng, H., Lee, W.C., Buza-Vidas, N., Nerlov, C., Jacobsen, S.E., Perry, P., Berry, R., Thornburn, A., et al. (2011). Acute multiple organ failure in adult mice deleted for the developmental regulator Wt1. *PLoS Genet.* 7, e1002404.
- Ciampi, O., Iacone, R., Longaretti, L., Benedetti, V., Graf, M., Magnone, M.C., Patsch, C., Xinaris, C., Remuzzi, G., Benigni, A., and Tomasoni, S. (2016). Generation of functional podocytes from human induced pluripotent stem cells. *Stem Cell Res.* 17, 130–139.
- Costantini, F., and Kopan, R. (2010). Patterning a complex organ: branching morphogenesis and nephron segmentation in kidney development. *Dev. Cell* 18, 698–712.
- Daehn, I., Casalena, G., Zhang, T., Shi, S., Fenninger, F., Barasch, N., Yu, L., D'Agati, V., Schlondorff, D., Kriz, W., et al. (2014). Endothelial mitochondrial oxidative stress determines podocyte depletion in segmental glomerulosclerosis. *J. Clin. Invest.* 124, 1608–1621.
- Davies, J.A., Ladomery, M., Hohenstein, P., Michael, L., Shafe, A., Spraggon, L., and Hastie, N. (2004). Development of an siRNA-based method for repressing specific genes in renal organ culture and its use to show that the Wt1 tumour suppressor is required for nephron differentiation. *Hum. Mol. Genet.* 13, 235–246.
- DeFilippis, M., and Wagner, K.D. (2014). Management of treatment-resistant depression in children and adolescents. *Paediatr. Drugs* 16, 353–361.
- Duim, S.N., Kurakula, K., Goumans, M.J., and Kruijthof, B.P. (2015). Cardiac endothelial cells express Wilms' tumor-1: Wt1 expression in the developing, adult and infarcted heart. *J. Mol. Cell. Cardiol.* 81, 127–135.
- Eng, D.G., Sunseri, M.W., Kaverina, N.V., Roeder, S.S., Pippin, J.W., and Shankland, S.J. (2015). Glomerular parietal epithelial cells contribute to adult podocyte regeneration in experimental focal segmental glomerulosclerosis. *Kidney Int.* 88, 999–1012.
- Essafi, A., Webb, A., Berry, R.L., Slight, J., Burn, S.F., Spraggon, L., Vecelela, V., Martinez-Estrada, O.M., Wiltshire, J.H., Roberts, S.G., et al. (2011). A wt1-controlled chromatin switching mechanism underpins tissue-specific wnt4 activation and repression. *Dev. Cell* 21, 559–574.
- Filipovic, N., Vukojevic, K., Bocina, I., Saraga, M., Durdov, M.G., Kablar, B., and Saraga-Babic, M. (2017). Immunohistochemical and electron microscopic features of mesenchymal-to-epithelial transition in human developing, postnatal and nephrotic podocytes. *Histochem. Cell Biol.* 147, 481–495.
- Gao, F., Maiti, S., Sun, G., Ordonez, N.G., Udtha, M., Deng, J.M., Behringer, R.R., and Huff, V. (2004). The Wt1+/R394W mouse displays glomerulosclerosis and early-onset renal failure characteristic of human Denys-Drash syndrome. *Mol. Cell. Biol.* 24, 9899–9910.
- Gomez, R.A., Belyea, B., Medrano, S., Pentz, E.S., and Sequeira-Lopez, M.L. (2014). Fate and plasticity of renin precursors in development and disease. *Pediatr. Nephrol.* 29, 721–726.
- Grahammer, F., Wanner, N., and Huber, T.B. (2013). Podocyte regeneration: who can become a podocyte? *Am. J. Pathol.* 183, 333–335.
- Graziano, A.C., Cardile, V., Avola, R., Vicario, N., Parenti, C., Salvatorelli, L., Magro, G., and Parenti, R. (2017). Wilms' tumor gene 1 silencing inhibits proliferation of human osteosarcoma MG-63 cell line by cell cycle arrest and apoptosis activation. *Oncotarget* 8, 13917–13931.
- Hodgin, J.B., Bitzer, M., Wickman, L., Afshinnia, F., Wang, S.Q., O'Connor, C., Yang, Y., Meadowbrooke, C., Chowdhury, M., Kikuchi, M., et al. (2015). Glomerular aging and focal global glomerulosclerosis: a podometric perspective. *J. Am. Soc. Nephrol.* 26, 3162–3178.
- Hohenstein, P., Pritchard-Jones, K., and Charlton, J. (2015). The yin and yang of kidney development and Wilms' tumors. *Genes Dev.* 29, 467–482.
- Ijpenberg, A., Perez-Pomares, J.M., Guadix, J.A., Carmona, R., Portillo-Sanchez, V., Macias, D., Hohenstein, P., Miles, C.M., Hastie, N.D., and Munoz-Chapuli, R. (2007). Wt1 and retinoic acid signaling are essential for stellate cell development and liver morphogenesis. *Dev. Biol.* 312, 157–170.
- Jomgeow, T., Oji, Y., Tsuji, N., Ikeda, Y., Ito, K., Tsuda, A., Nakazawa, T., Tatsumi, N., Sakaguchi, N., Takashima, S., et al. (2006). Wilms' tumor gene WT1 17AA(-)/KTS(-) isoform induces morphological changes and promotes cell migration and invasion in vitro. *Cancer Sci.* 97, 259–270.
- Kann, M., Ettou, S., Jung, Y.L., Lenz, M.O., Taglienti, M.E., Park, P.J., Schermer, B., Benzing, T., and Kreidberg, J.A. (2015). Genome-wide analysis of Wilms' tumor 1-controlled gene expression in podocytes reveals key regulatory mechanisms. *J. Am. Soc. Nephrol.* 26, 2097–2104.
- Karki, S., Surolia, R., Hock, T.D., Guroji, P., Zolak, J.S., Duggal, R., Ye, T., Thannickal, V.J., and Antony, V.B. (2014). Wilms' tumor 1 (Wt1) regulates pleural mesothelial cell plasticity and transition



- into myofibroblasts in idiopathic pulmonary fibrosis. *FASEB J.* 28, 1122–1131.
- Kaverina, N.V., Eng, D.G., Schneider, R.R., Pippin, J.W., and Shankland, S.J. (2016). Partial podocyte replenishment in experimental FSGS derives from nonpodocyte sources. *Am. J. Physiol. Renal Physiol.* 310, F1397–F1413.
- Kimura, K., Nagai, R., Sakai, T., Aikawa, M., Kuro-o, M., Kobayashi, N., Shirato, I., Inagami, T., Oshi, M., Suzuki, N., et al. (1995). Diversity and variability of smooth muscle phenotypes of renal arterioles as revealed by myosin isoform expression. *Kidney Int.* 48, 372–382.
- Kobayashi, A., Valerius, M.T., Mugford, J.W., Carroll, T.J., Self, M., Oliver, G., and McMahon, A.P. (2008). Six2 defines and regulates a multipotent self-renewing nephron progenitor population throughout mammalian kidney development. *Cell Stem Cell* 3, 169–181.
- Kuppe, C., Grone, H.J., Ostendorf, T., van Kuppevelt, T.H., Boor, P., Floege, J., Smeets, B., and Moeller, M.J. (2015). Common histological patterns in glomerular epithelial cells in secondary focal segmental glomerulosclerosis. *Kidney Int.* 88, 990–998.
- Lasagni, L., Lazzeri, E., Shankland, S.J., Anders, H.J., and Romagnani, P. (2013). Podocyte mitosis - a catastrophe. *Curr. Mol. Med.* 13, 13–23.
- Lasagni, L., Angelotti, M.L., Ronconi, E., Lombardi, D., Nardi, S., Peired, A., Becherucci, F., Mazzinghi, B., Sisti, A., Romoli, S., et al. (2015). Podocyte regeneration driven by renal progenitors determines glomerular disease remission and can be pharmacologically enhanced. *Stem Cell Reports* 5, 248–263.
- Lazzeri, E., and Romagnani, P. (2015). Podocyte biology: differentiation of parietal epithelial cells into podocytes. *Nat. Rev. Nephrol.* 11, 7–8.
- Li, X., Ottosson, S., Wang, S., Jernberg, E., Boldrup, L., Gu, X., Nylander, K., and Li, A. (2015). Wilms' tumor gene 1 regulates p63 and promotes cell proliferation in squamous cell carcinoma of the head and neck. *BMC Cancer* 15, 342.
- Lichtnekert, J., Kaverina, N.V., Eng, D.G., Gross, K.W., Kutz, J.N., Pippin, J.W., and Shankland, S.J. (2016). Renin-angiotensin-aldosterone system inhibition increases podocyte derivation from cells of renin lineage. *J. Am. Soc. Nephrol.* 27, 3611–3627.
- Little, M.H., and McMahon, A.P. (2012). Mammalian kidney development: principles, progress, and projections. *Cold Spring Harb. Perspect. Biol.* 4, 1–46.
- Marshall, C.B., Krofft, R.D., Blonski, M.J., Kowalewska, J., Logar, C.M., Pippin, J.W., Kim, F., Feil, R., Alpers, C.E., and Shankland, S.J. (2011). Role of smooth muscle protein SM22alpha in glomerular epithelial cell injury. *Am. J. Physiol. Renal Physiol.* 300, F1026–F1042.
- Martinez-Estrada, O.M., Lettice, L.A., Essafi, A., Guadix, J.A., Slight, J., Velecela, V., Hall, E., Reichmann, J., Devenney, P.S., Hohenstein, P., et al. (2010). Wt1 is required for cardiovascular progenitor cell formation through transcriptional control of Snail and E-cadherin. *Nat. Genet.* 42, 89–93.
- Matsushita, K., Morello, F., Wu, Y., Zhang, L., Iwanaga, S., Pratt, R.E., and Dzau, V.J. (2010). Mesenchymal stem cells differentiate into renin-producing juxtaglomerular (JG)-like cells under the control of liver X receptor-alpha. *J. Biol. Chem.* 285, 11974–11982.
- Mazzei, L., and Manucha, W. (2016). Growing evidence suggests WT1 effects in the kidney development are modulated by Hsp70/NO interaction. *J. Nephrol.* 1, 1–18.
- Miller-Hodges, E., and Hohenstein, P. (2012). WT1 in disease: shifting the epithelial-mesenchymal balance. *J. Pathol.* 226, 229–240.
- Ohse, T., Vaughan, M.R., Kopp, J.B., Krofft, R.D., Marshall, C.B., Chang, A.M., Hudkins, K.L., Alpers, C.E., Pippin, J.W., and Shankland, S.J. (2010). De novo expression of podocyte proteins in parietal epithelial cells during experimental glomerular disease. *Am. J. Physiol. Renal Physiol.* 298, F702–F711.
- Ozdemir, D.D., and Hohenstein, P. (2014). Wt1 in the kidney—a tale in mouse models. *Pediatr. Nephrol.* 29, 687–693.
- Pavenstadt, H., Kriz, W., and Kretzler, M. (2003). Cell biology of the glomerular podocyte. *Physiol. Rev.* 83, 253–307.
- Pelletier, J., Bruening, W., Kashtan, C.E., Mauer, S.M., Manivel, J.C., Striegel, J.E., Houghton, D.C., Junien, C., Habib, R., Fouser, L., et al. (1991). Germline mutations in the Wilms' tumor suppressor gene are associated with abnormal urogenital development in Denys-Drash syndrome. *Cell* 67, 437–447.
- Petermann, A.T., Krofft, R., Blonski, M., Hiromura, K., Vaughn, M., Pichler, R., Griffin, S., Wada, T., Pippin, J., Durvasula, R., and Shankland, S.J. (2003). Podocytes that detach in experimental membranous nephropathy are viable. *Kidney Int.* 64, 1222–1231.
- Pippin, J.W., Sparks, M.A., Glenn, S.T., Buitrago, S., Coffman, T.M., Duffield, J.S., Gross, K.W., and Shankland, S.J. (2013). Cells of renin lineage are progenitors of podocytes and parietal epithelial cells in experimental glomerular disease. *Am. J. Pathol.* 183, 542–557.
- Pippin, J.W., Glenn, S.T., Krofft, R.D., Rusiniak, M.E., Alpers, C.E., Hudkins, K., Duffield, J.S., Gross, K.W., and Shankland, S.J. (2014). Cells of renin lineage take on a podocyte phenotype in aging nephropathy. *Am. J. Physiol. Renal Physiol.* 306, F1198–F1209.
- Pippin, J.W., Kaverina, N.V., Eng, D.G., Krofft, R.D., Glenn, S.T., Duffield, J.S., Gross, K.W., and Shankland, S.J. (2015). Cells of renin lineage are adult pluripotent progenitors in experimental glomerular disease. *Am. J. Physiol. Renal Physiol.* 309, F341–F358.
- Puelles, V.G., Douglas-Denton, R.N., Cullen-McEwen, L.A., Li, J., Hughson, M.D., Hoy, W.E., Kerr, P.G., and Bertram, J.F. (2015). Podocyte number in children and adults: associations with glomerular size and numbers of other glomerular resident cells. *J. Am. Soc. Nephrol.* 26, 2277–2288.
- Romagnani, P. (2011). Parietal epithelial cells: their role in health and disease. *Contrib. Nephrol.* 169, 23–36.
- Romagnani, P., Lasagni, L., and Remuzzi, G. (2013). Renal progenitors: an evolutionary conserved strategy for kidney regeneration. *Nat. Rev. Nephrol.* 9, 137–146.
- Ronconi, E., Sagrinati, C., Angelotti, M.L., Lazzeri, E., Mazzinghi, B., Ballerini, L., Parente, E., Becherucci, F., Gacci, M., Carini, M., et al. (2009). Regeneration of glomerular podocytes by human renal progenitors. *J. Am. Soc. Nephrol.* 20, 322–332.
- Sequeira Lopez, M.L., Pentz, E.S., Robert, B., Abrahamson, D.R., and Gomez, R.A. (2001). Embryonic origin and lineage of juxtaglomerular cells. *Am. J. Physiol. Renal Physiol.* 281, F345–F356.



- Sequeira Lopez, M.L., Pentz, E.S., Nomasa, T., Smithies, O., and Gomez, R.A. (2004). Renin cells are precursors for multiple cell types that switch to the renin phenotype when homeostasis is threatened. *Dev. Cell* 6, 719–728.
- Shankland, S.J., Pippin, J.W., and Duffield, J.S. (2014). Progenitor cells and podocyte regeneration. *Semin. Nephrol.* 34, 418–428.
- Starke, C., Betz, H., Hickmann, L., Lachmann, P., Neubauer, B., Kopp, J.B., Sequeira-Lopez, M.L., Gomez, R.A., Hohenstein, B., Todorov, V.T., and Hugo, C.P. (2015). Renin lineage cells repopulate the glomerular mesangium after injury. *J. Am. Soc. Nephrol.* 26, 48–54.
- Steege, A., Fahling, M., Paliege, A., Bondke, A., Kirschner, K.M., Martinka, P., Kaps, C., Patzak, A., Persson, P.B., Thiele, B.J., et al. (2008). Wilms' tumor protein (-KTS) modulates renin gene transcription. *Kidney Int.* 74, 458–466.
- Stefanska, A., Peault, B., and Mullins, J.J. (2013). Renal pericytes: multifunctional cells of the kidneys. *Pflugers Arch.* 465, 767–773.
- Stefanska, A., Eng, D., Kaverina, N., Pippin, J.W., Gross, K.W., Duffield, J.S., and Shankland, S.J. (2016). Cells of renin lineage express hypoxia inducible factor 2alpha following experimental ureteral obstruction. *BMC Nephrol.* 17, 1–29.
- Thoma, C. (2014). Glomerular disease: to the rescue—migrating renin lineage cells heal the injured glomerular mesangium. *Nat. Rev. Nephrol.* 10, 424.
- Tretiakova, M., and Hart, J. (2011). Laser microdissection for gene expression study of hepatocellular carcinomas arising in cirrhotic and non-cirrhotic livers. *Methods Mol. Biol.* 755, 233–244.
- Wagner, N., Michiels, J.F., Schedl, A., and Wagner, K.D. (2008). The Wilms' tumour suppressor WT1 is involved in endothelial cell proliferation and migration: expression in tumour vessels in vivo. *Oncogene* 27, 3662–3672.
- Wagner, K.D., Cherfils-Vicini, J., Hosen, N., Hohenstein, P., Gilson, E., Hastie, N.D., Michiels, J.F., and Wagner, N. (2014). The Wilms' tumour suppressor Wt1 is a major regulator of tumour angiogenesis and progression. *Nat. Commun.* 5, 5852.
- Wang, H., Gomez, J.A., Klein, S., Zhang, Z., Seidler, B., Yang, Y., Schmeckpeper, J., Zhang, L., Muramoto, G.G., Chute, J., et al. (2013). Adult renal mesenchymal stem cell-like cells contribute to juxtaglomerular cell recruitment. *J. Am. Soc. Nephrol.* 24, 1263–1273.
- Wanner, N., Hartleben, B., Herbach, N., Goedel, M., Stickel, N., Zeiser, R., Walz, G., Moeller, M.J., Grahammer, F., and Huber, T.B. (2014). Unraveling the role of podocyte turnover in glomerular aging and injury. *J. Am. Soc. Nephrol.* 25, 707–716.
- Wen, Q., Wang, Y., Tang, J., Cheng, C.Y., and Liu, Y.X. (2016). Sertoli cell Wt1 regulates peritubular myoid cell and fetal Leydig cell differentiation during fetal testis development. *PLoS One* 11, e0167920.
- Wu, C., Wang, S., Xu, C., Tyler, A., Li, X., Andersson, C., Oji, Y., Sugiyama, H., Chen, Y., and Li, A. (2015). WT1 enhances proliferation and impedes apoptosis in KRAS mutant NSCLC via targeting cMyc. *Cell Physiol. Biochem.* 35, 647–662.
- Zhang, J., Pippin, J.W., Krofft, R.D., Naito, S., Liu, Z.H., and Shankland, S.J. (2013). Podocyte repopulation by renal progenitor cells following glucocorticoids treatment in experimental FSGS. *Am. J. Physiol. Renal Physiol.* 304, F1375–F1389.
- Zhang, J., Yanez, D., Floege, A., Lichtnekert, J., Krofft, R.D., Liu, Z.H., Pippin, J.W., and Shankland, S.J. (2015). ACE-inhibition increases podocyte number in experimental glomerular disease independent of proliferation. *J. Renin Angiotensin Aldosterone Syst.* 16, 234–248.

**Stem Cell Reports, Volume 9**

**Supplemental Information**

**WT1 Is Necessary for the Proliferation and Migration of Cells of Renin  
Lineage Following Kidney Podocyte Depletion**

**Natalya V. Kaverina, Diana G. Eng, Andrea D. Largent, Ilse Daehn, Anthony  
Chang, Kenneth W. Gross, Jeffrey W. Pippin, Peter Hohenstein, and Stuart J. Shankland**

Supplemental Figures

Figure S1

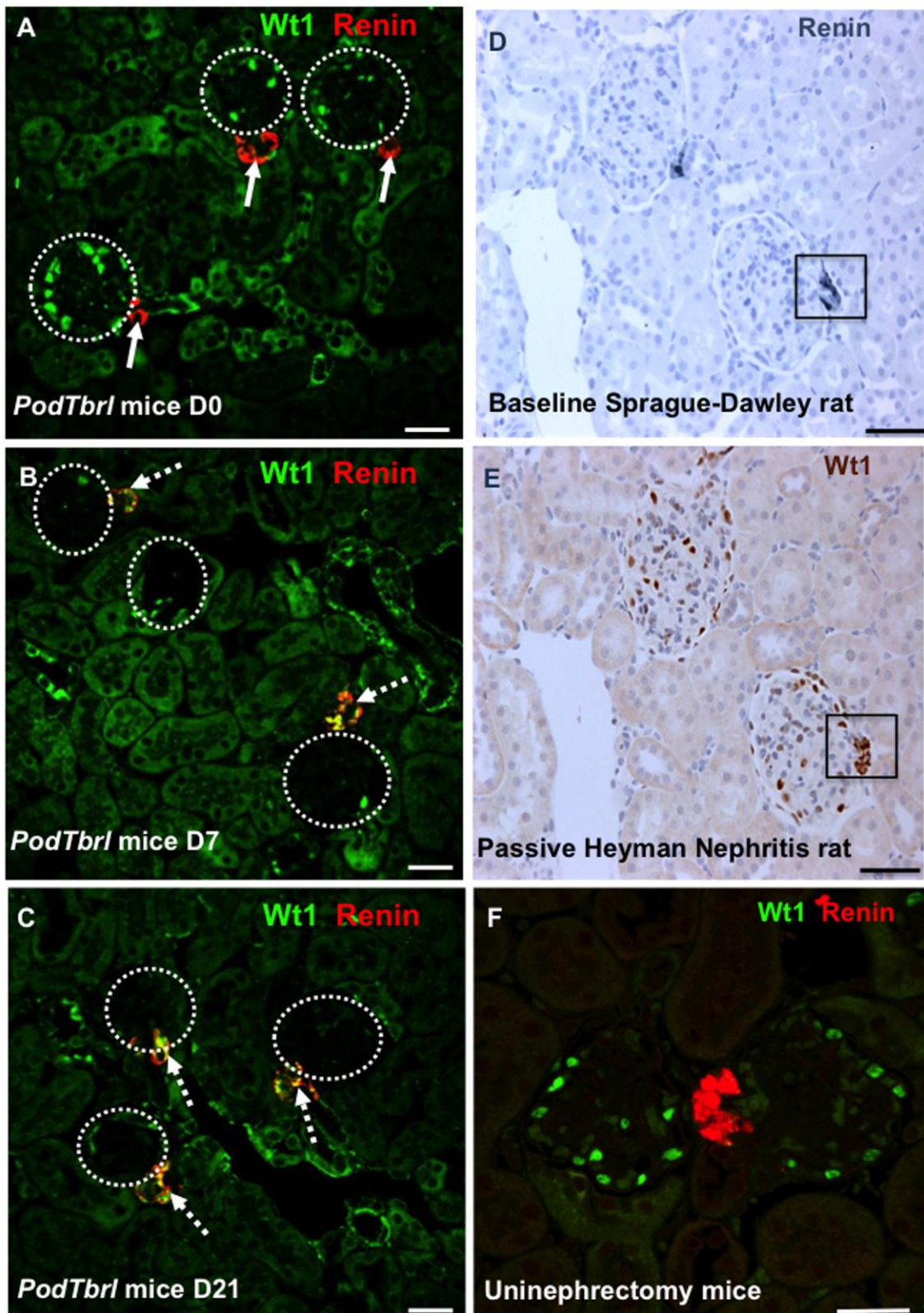


**Figure S1:** *WT1 staining is increased in renin-expressing cells following podocyte depletion in podocyte TGF $\beta$ -Receptor1 transgenic mice and the passive Heymann nephritis model, but not in the uninephrectomy model of glomerular hypertrophy.*

(A-C) *Podocyte TGF $\beta$ -Receptor1 transgenic (PodTgfr1) mice:* Representative two-color immunofluorescence double staining of WT1 (green) and Renin (red, solid arrow). The outline of glomeruli is shown with dashed circles. (A) At D0 in mice not given doxycycline, renin was confined to the juxta-glomerular compartment (JGC), and WT1 to glomeruli, hence there was no overlap. (B) Decreased glomerular WT1 staining represents marked podocyte depletion at D7 after doxycycline induction. WT1 staining is increased in renin-expressing cells (yellow color marked with dashed arrows). (C). At D21, podocyte depletion was persistent. WT1 staining merges with RFP cells in the JGC.

Scale bars represent 20 $\mu$ m.

(D, E) *PHN model of membranous nephropathy.* Two sequential kidney sections (4 $\mu$ m thick) were stained with renin (dark blue) and WT1 (brown) respectively. renin stained cells marked with solid boxes in the JGC (D) co-stain for WT1 (E). Scale bars represent 20 $\mu$ m.

(F) *Uninephrectomy model.* Double immunofluorescence shows that WT1 (green) and renin (red) do not colocalize (no yellow color) in this model where absolute podocyte number is unchanged. Scale bars represent 20 $\mu$ m.

Figure S2

Kaverina et al.

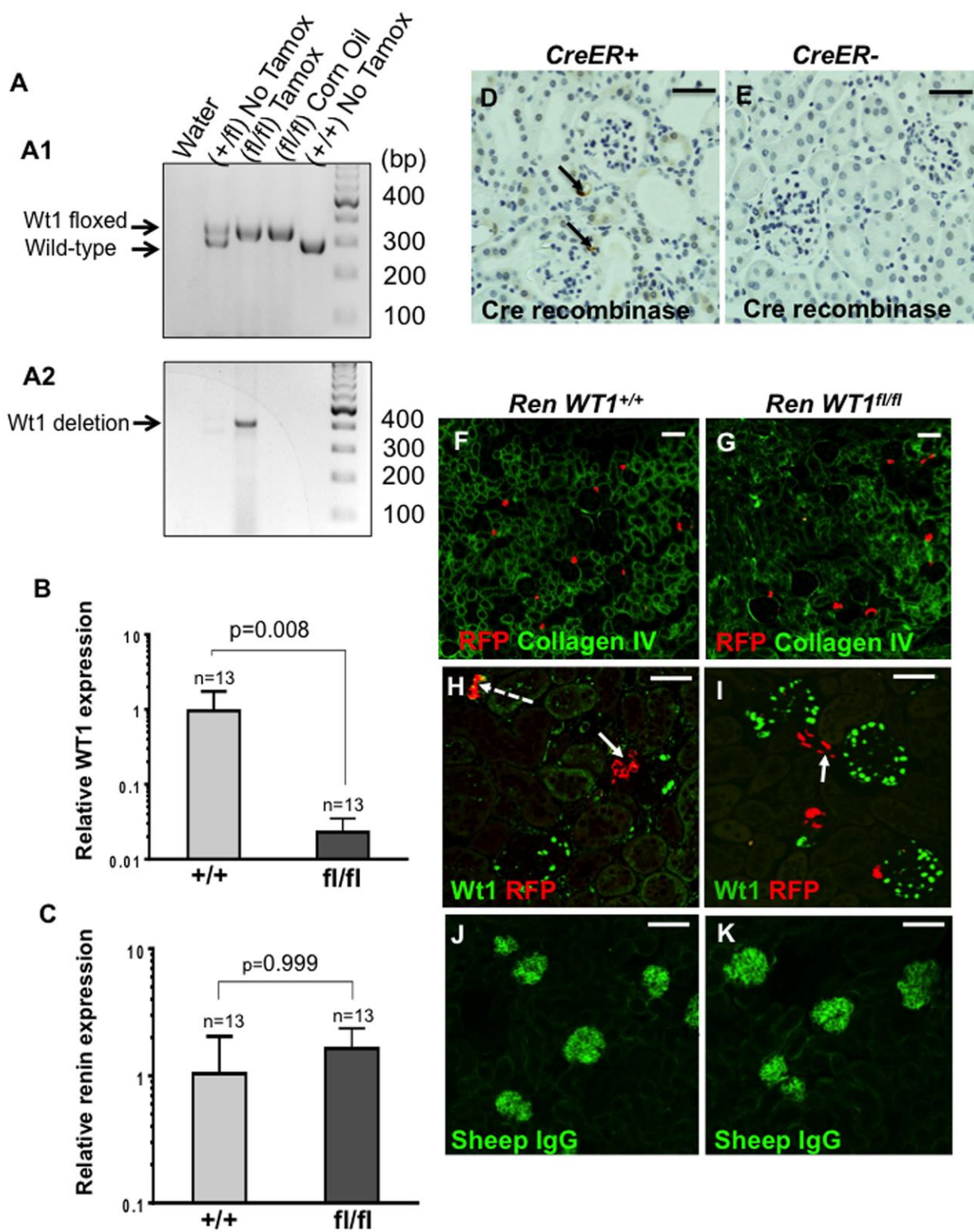


**Figure S2: Characterization of *RenWt1*<sup>+/+</sup> and *RenWt1*<sup>fl/fl</sup> reporter mice.**

(A) *Genotyping*: (A1) Tail snip DNA was used for PCR to identify animals that carried CreER, and either the wildtype (327bp) or floxed Wt1 (300bp) alleles. DNA loaded from left to right includes no DNA (water), *RenWt1*<sup>+/fl</sup> no tamoxifen (tamox), *RenWt1*<sup>fl/fl</sup> administered tamox, *RenWt1*<sup>fl/fl</sup> administered vehicle (corn oil), and *RenWt1*<sup>+/+</sup> no tamox. (A2) DNA isolated from kidney cortex from the above animals underwent PCR to verify the Cre-mediated deletion of the floxed Wt1 (420bp) in *RenWt1*<sup>fl/fl</sup> animals given tamox. As expected, animals not given tamoxifen did not show a flox deletion band.

(B, C) *Relative mRNA expression*: qPCR of mRNA from laser captured RFP positive cells in the juxta-glomerular compartment from *RenWt1*<sup>+/+</sup> and *RenWt1*<sup>fl/fl</sup> mice given tamox. (B) Relative Wt1 expression is significantly less in *RenWt1*<sup>fl/fl</sup> animals. (C) There is no significant differences in renin mRNA in the same samples (n=13/per group)

(D, E) *Cre recombinase staining* is detected in the JGC of CreER positive animals (arrow), but not in cre negative animals as expected. Scale bars represent 20μm.

(F, G) *Reporting*: Collagen IV (green) was used to delineate glomeruli. Low power view shows that tdTomato reporter (red) was similar in *RenWt1*<sup>+/+</sup> and *RenWt1*<sup>fl/fl</sup> mice given tamoxifen. Scale bars represent 50μm.

(H, I) *WT1 staining*: In baseline *RenWt1*<sup>+/+</sup> mice, WT1 staining (green) is co-expressed in less than 5% of RFP<sup>+</sup> cells (red, solid arrows), creating a yellow color (dashed arrow). WT1 staining is not detected in RFP cells in *RenWt1*<sup>fl/fl</sup> mice. Scale bars represent 20μm.

(J, K) *Sheep IgG staining*: used to determine deposition of the cytotopathic anti-podocyte antibody to induce podocyte loss, was similar in *RenWt1*<sup>+/+</sup> and *RenWt1*<sup>fl/fl</sup> mice. Scale bars represent 40μm.

Figure S3

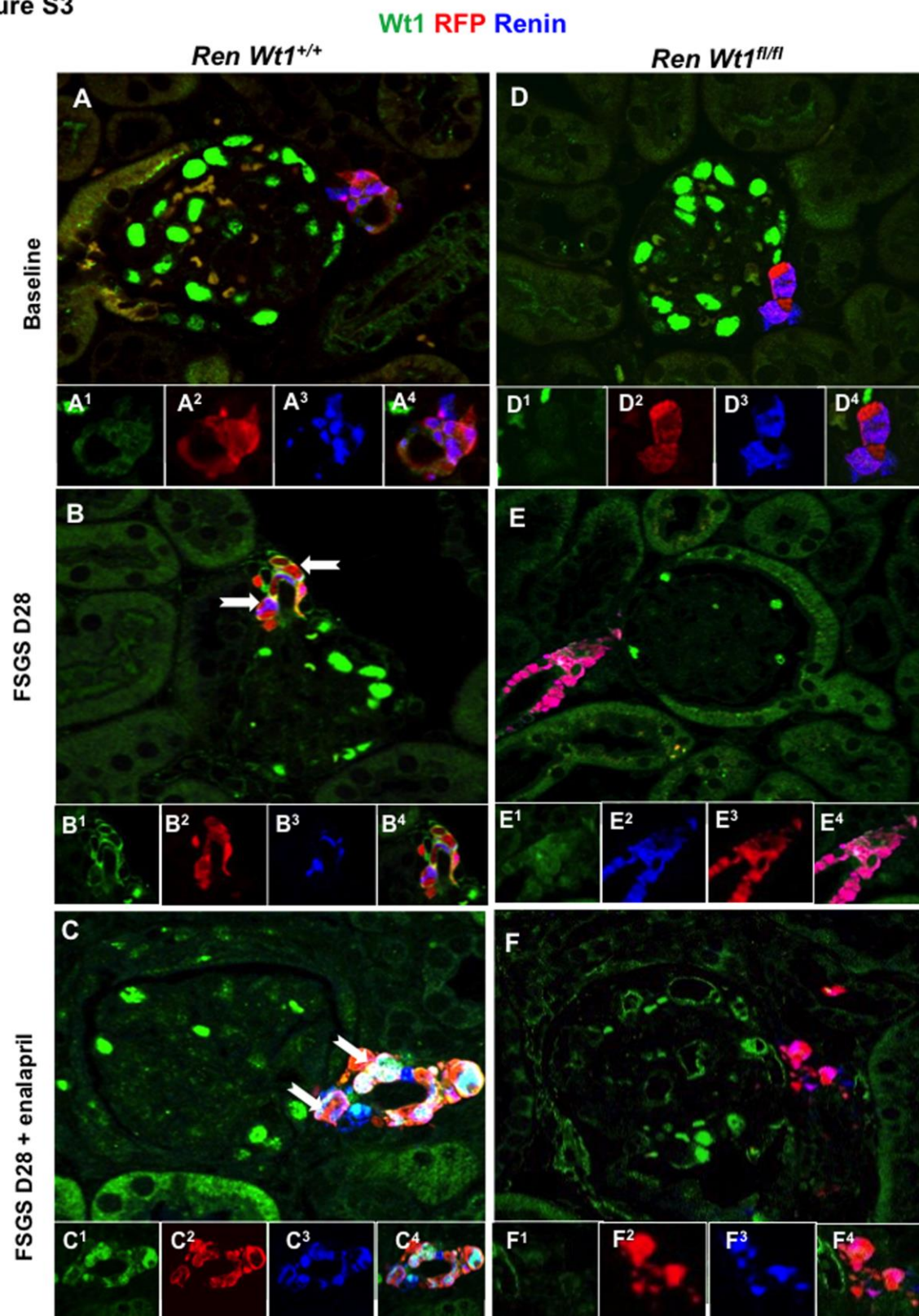


**Figure S3:** *Cells of renin lineage (CoRL) co-expressing renin and WT1 in RenWt1<sup>+/+</sup> mice following podocyte depletion in the cytotoxic anti-podocyte antibody model of FSGS.*

(A-F) Triple staining was performed with antibodies to WT1 (green), red fluorescent protein (RFP, red) and renin (blue) in *RenWt1<sup>+/+</sup>* and *RenWt1<sup>fl/fl</sup>* mice, and imaged using confocal microscopy. The larger pictures show the merge of all three colors; individual panels labeled 1-4 show individual colors for WT1, RFP, renin and their merge respectively. A merge of RFP, WT1 and renin creates a white color (B, C) (marked with solid arrows), and a merge of RFP and renin creates a purple color (A, D-F) (marked with dashed arrows).

In baseline *RenWt1<sup>+/+</sup>* (A) and *RenWt1<sup>fl/fl</sup>* (D) mice, WT1 staining was readily detected in podocytes; RFP and staining was restricted to the juxta-glomerulus compartment (JGC), and were indistinguishable at baseline. (B) At FSGS D28 in *RenWt1<sup>+/+</sup>* mice, WT1 staining was detected in RFP<sup>+</sup>CoRL in the JGC (marked with solid arrows). (E) WT1<sup>+</sup>RFP<sup>+</sup> staining was not detected in *RenWt1<sup>fl/fl</sup>* mice at FSGS D28. The number of podocytes staining for WT1 was reduced in both strains at FSGS D28, but was more severe in diseased *RenWt1<sup>fl/fl</sup>* mice. (C) Giving Enalapril to diseased *RenWt1<sup>+/+</sup>* mice augmented WT1 expression in RFP<sup>+</sup>CoRL (marked with solid arrow), but not in diseased *RenWt1<sup>fl/fl</sup>* mice (F).

Figure S4

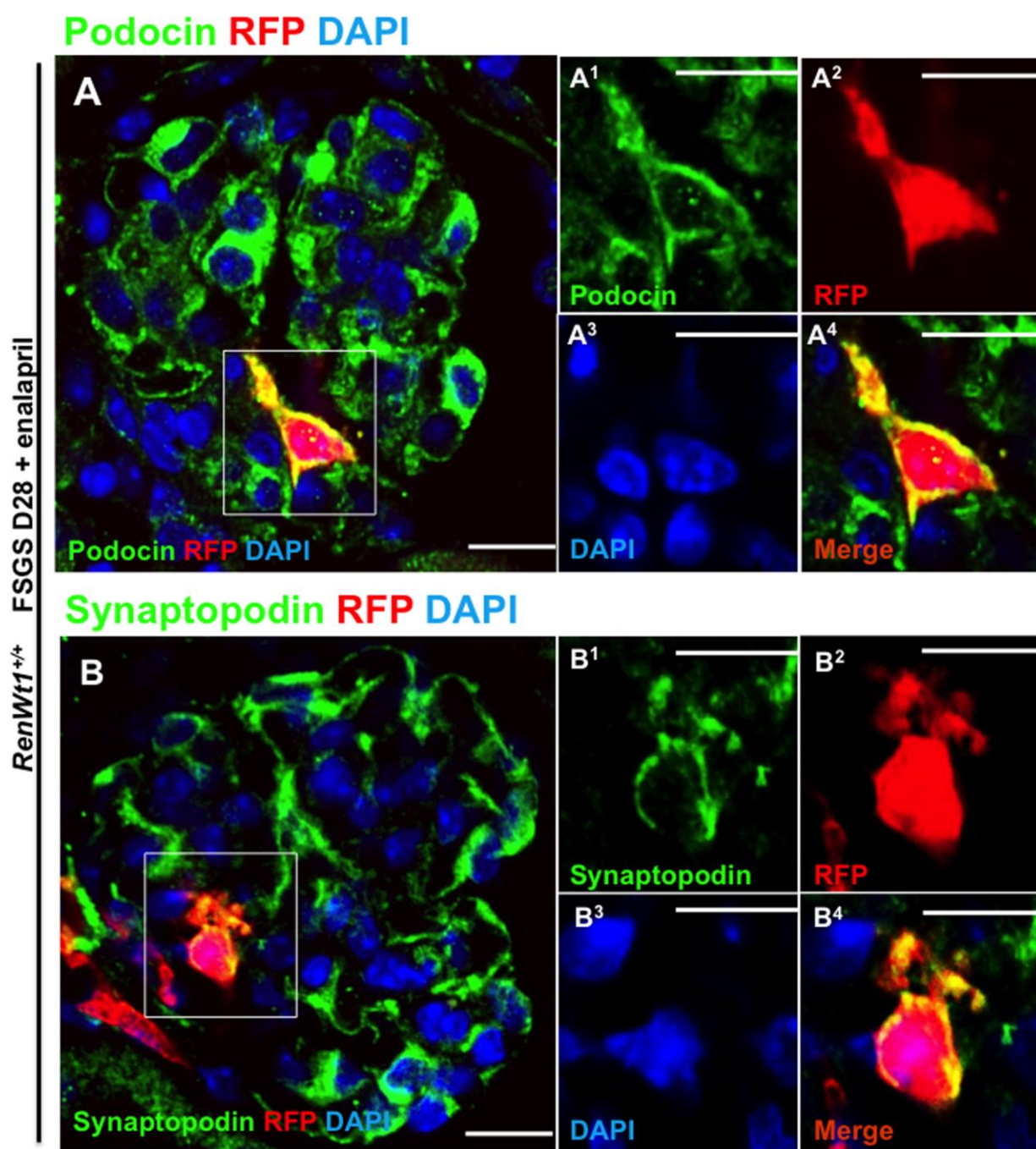


**Figure S4:** *Cells of renin lineage (CoRL) begin to de novo express the podocyte markers in enalapril treated RenWt1<sup>+/+</sup> mice at D28 of FSGS following podocyte depletion.*

(A) Representative image of three color staining for podocin (podocyte marker, green), RFP identifies td-Tomato-labeled CoRL, red) and DAPI.(nuclear, blue). (A1-A4) Insets show images of individual colors for podocin, RFP, DAPI and their merge respectively of CoRL in the glomerular tuft. Podocin (A1) co-localized with RFP+CoRL (A2) merging as yellow color (A4) with corresponding nuclear staining (A3)

(B) Representative image of three color staining for synaptopodin (podocyte marker, green), RFP identifies td-Tomato-labeled CoRL, red) and DAPI.(nuclear, blue). (B1- B4) Insets show images of individual colors for synaptopodin, RFP, DAPI and their merge respectively of CoRL in the glomerular tuft. Synaptopodin (B1) co-localized with RFP+CoRL (B2) merging as yellow color (B4) with corresponding nuclear staining (B3) Scale bars represent 20µm.

Figure S5

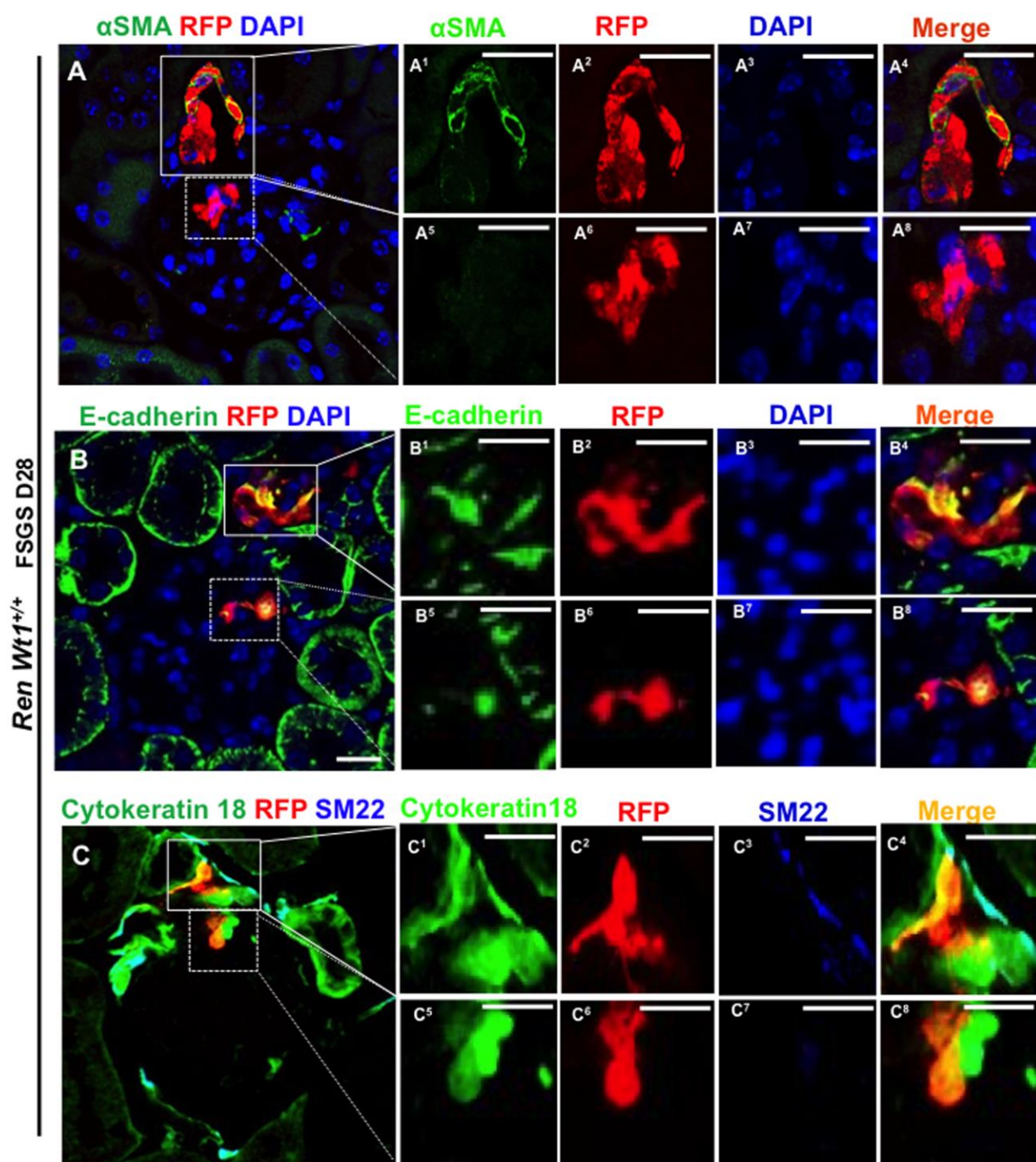


**Figure S5:** *Following podocyte depletion in the cytotoxic anti-podocyte antibody model, cells of renin lineage (CoRL) that migrate from the juxtaglomerular compartment (JGC) to the glomerulus de novo express epithelial markers, and no longer express mesenchymal markers.*

**(A)** *Loss of mesenchymal marker when CoRL migrates to glomerulus following podocyte depletion.* Confocal images shows three color staining for  $\alpha$ SMA (mesenchymal marker, green), RFP (labeled CoRL, red) and DAPI (nuclear, blue). Solid box indicates the JGC, dashed box indicates CoRL in the glomerular tuft. Higher magnification views of individual stains labeled as superscripted panels 1-4. In the JGC,  $\alpha$ SMA (**A1**) is constitutively expressed in RFP<sup>+</sup>CoRL (**A2**), merging as a yellow/ orange color (**A4**) with corresponding nuclear staining (**A3**). In contrast,  $\alpha$ SMA staining (**A5**) is not detected in a RFP<sup>+</sup> cell in the glomerular tuft (**A6**), and thus no merge (**A8**).

**(B)** *De novo staining for an epithelial cell marker in the JGC persists when CoRL migrates to the glomerulus.* Confocal microscopy shows staining for E-cadherin (epithelial marker, green), RFP (CoRL, red) and DAPI (nuclear, blue) in the JGC (solid inset) and glomerular tuft (dashed inset) at D28. In the JGC, there is de novo staining for E-cadherin (green, **B1**) that co-localizes with RFP (**B2**), to create a merged yellow/orange color (**B4**). In the glomerulus, E-cadherin staining persists (**B5**) in an RFP<sup>+</sup> cell (**B6**) to create a yellow/orange color (**B8**).

**(C)** *In the glomerulus, a migrated CoRL loses mesenchymal markers while de novo expressing epithelial marker.* Confocal microscopy shows staining for SM22 (mesenchymal marker, blue), Cytokeratin 18 (epithelial marker, green) RFP (identifies CoRL, red). JGC and glomerular tuft shown with solid and dashed insets respectively. In the JGC following podocyte depletion, RFP<sup>+</sup> cells (**C2**) co-express cytokeratin 18 (**C1**) and SM22 (**C3**) to merge as a light blue color (**C4**). In the glomerulus, an RFP<sup>+</sup> cell (**C5**), co-expresses cytokeratin 18, but no longer expresses SM22, to create a yellow color (**C8**). Scale bars represent 20 $\mu$ m.

Figure S6

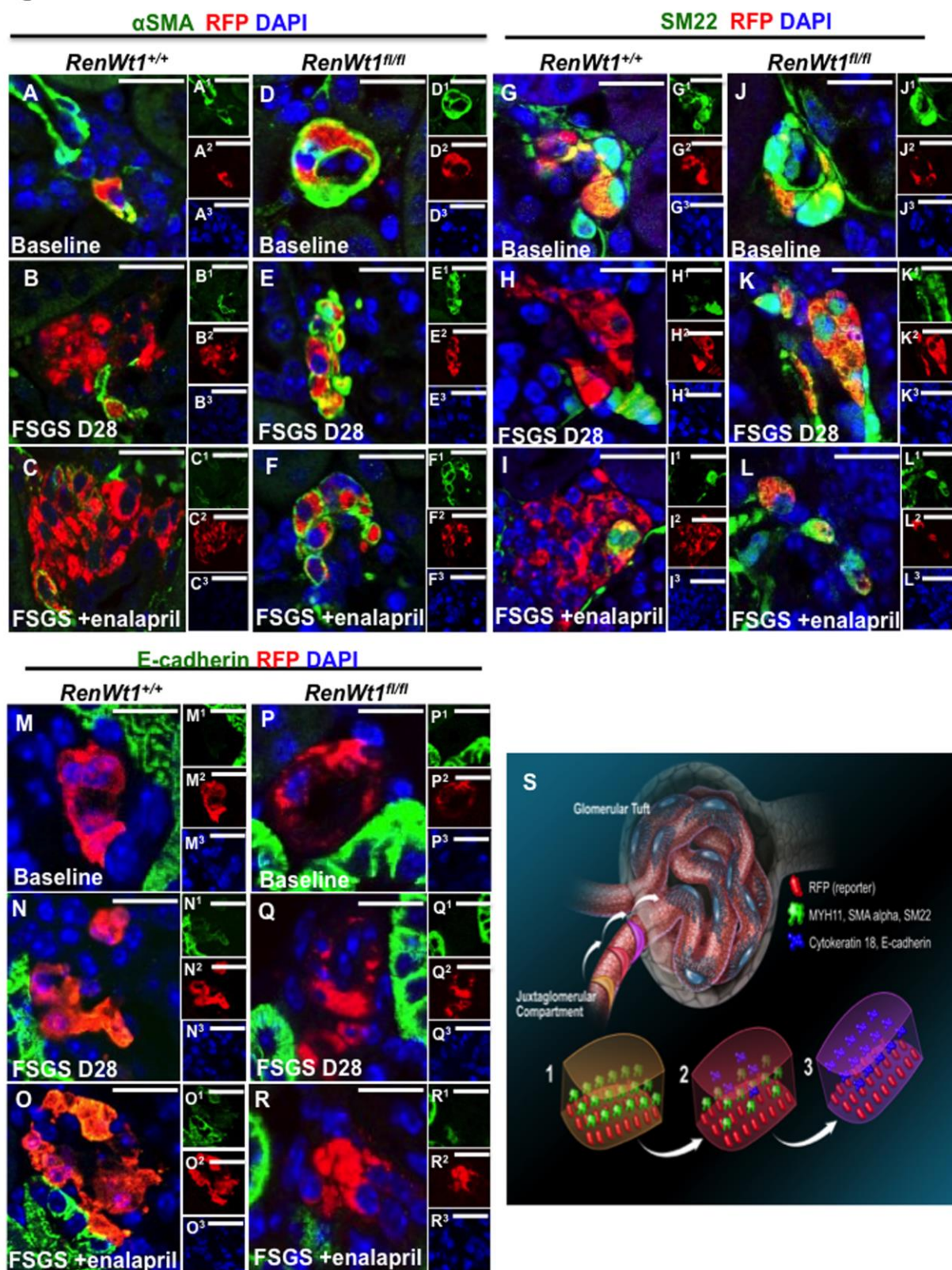


**Figure S6:** *Following podocyte depletion, cells of renin lineage (CoRL) in the juxta-glomerular compartment (JGC) have reduced staining for mesenchymal markers, but increased staining for epithelial cells markers.*

(A-F) Images are limited to the JGC, showing the mesenchymal marker  $\alpha$ SMA (green) and RFP (red) co-staining with DAPI counterstain (blue). Individual insets labeled by superscript show individual stains. Scale bars represent 20 $\mu$ m.

(A-C) *RenWt1*<sup>+/+</sup> mice. (A) At baseline,  $\alpha$ SMA (A1) is readily detected in RFP cells (A2) in the JGC, merging to create a yellow color. (B) At D28 FSGS,  $\alpha$ SMA staining is reduced (B1) in RFP cells (B2) that have increased in number. (C) At D28 with enalapril,  $\alpha$ SMA staining (C1) is markedly reduced in RFP cells (C2), leading to very little if any merged color due to a decrease in staining of  $\alpha$ SMA in RFP cells.

(D-F) *RenWt1*<sup>fl/fl</sup> mice. (D) At baseline,  $\alpha$ SMA staining (D1) overlaps with RFP (D2) to create a yellow color in cells of the JGC. (E, F) At D28 FSGS and D28 with enalapril,  $\alpha$ SMA staining (E1, F1) remains unchanged from baseline in RFP cells (E2, F2).

(G-L) Co-staining for the mesenchymal marker SM22 (green) and RFP (red) in cells of the JGC, counterstained with DAPI (blue). Scale bars represent 20 $\mu$ m. (G-I) *RenWt*<sup>+/+</sup> mice. (G) At baseline, SM22 staining (G1) is abundant in RFP cells (G2), merging to create a yellow color. (H) At FSGS D28, SM22 staining decreases (H1) in RFP cells (H2), leading to less merge evidenced by less yellow color. (I) At D28 plus enalapril, SM22 staining decreases markedly (I1), although the number of RFP cells (I2) increases.

(J-L) *RenWt1*<sup>fl/fl</sup> mice. SM22 staining is readily detected in RFP cells in the JGC creating a yellow color at baseline (J), which is unchanged at D28 FSGS (K) and D28 FSGS with Enalapril (L).

(M-R) Co-staining for the epithelial cell marker E-cadherin (green) and RFP (red) in cells of the JGC, counterstained with DAPI (blue). Scale bars represent 20 $\mu$ m. (M-O) *RenWt*<sup>+/+</sup> mice. (M) At baseline, E-cadherin staining (M1) is detected in the tubules, but not in RFP cells (M2) in the JGC. (N) At D28 FSGS, de novo E-cadherin staining (N1) is detected in RFP cells (N2), creating a yellow color. (O) In FSGS mice given enalapril, de novo E-cadherin staining is abundant (O1) in RFP cells (O2).

(P-R) *RenWt1*<sup>fl/fl</sup> mice. The epithelial marker E-cadherin is not expressed in RFP cells at baseline (P), D28 FSGS (Q) and D28 enalapril treated FSGS mice (R).

(S) Schema depicting CoRL mesenchymal-to-epithelial transition in *Wt1* wildtype mice with FSGS

Within the juxtaglomerular compartment, 1.) demonstrates the expression of the tdTomato reporter, detected by an antibody to RFP (indicated by the red bodies) and mesenchymal markers  $\alpha$ SMA, MYH11, SM22 (indicated by the green bodies) 2.) Following podocyte depletion, RFP is maintained, however the mesenchymal markers decrease, as epithelial markers (indicated by the blue bodies) begin to increase. 3.) As MET progresses, RFP continues to be maintained, while the mesenchymal markers are absent and epithelial markers are expressed. Cells that migrate to glomerular tuft undergo to MET-like changes.

Figure S7

Cytotoxic Anti-Podocyte Antibody Model

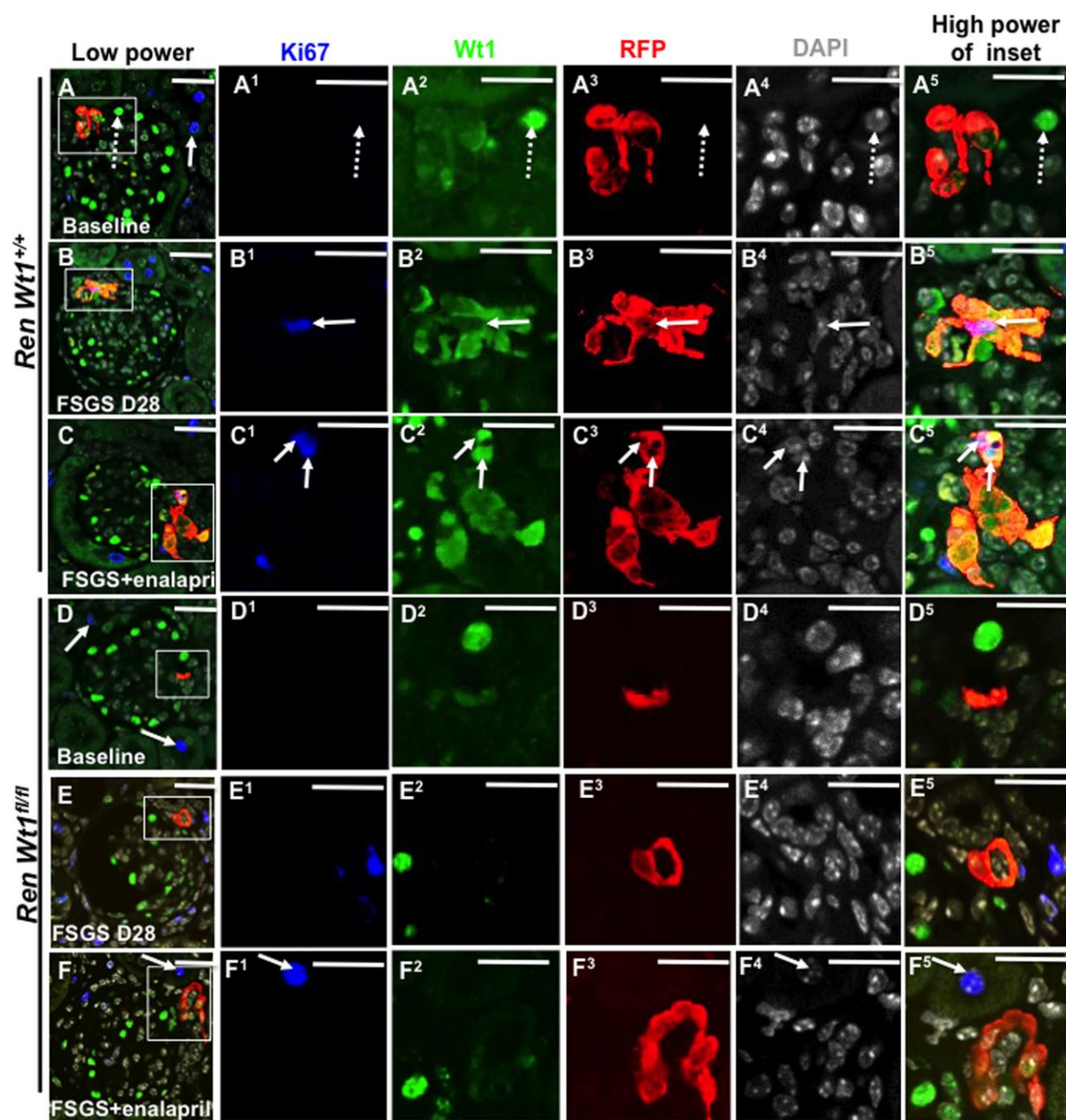


**Figure S7: Following podocyte depletion in the cytotoxic anti-podocyte antibody model of FSGS, Ki67 is detected in WT1 stained cells of renin lineage.**

Confocal images of Ki67 (blue), WT1 (green), RFP (red) and DAPI (grey). Insets show the JGC, and the individual antibody panels from the inset are shown as enlarged pictures.

(A-C) *RenWt1<sup>+/+</sup>* mice. (A) At baseline, Ki67 (A1) is not detected in the JGC, but is detected in neighboring tubules (solid arrow). WT1 staining (A2) is not detected in RFP cells (A3), but is positive in neighboring podocyte (dashed arrow). (B) At D28, Ki67 (B1, solid arrow) is detected in WT1 stained cells (B2) that co-localizes with RFP (B3). The triple merge (Ki67, WT1, RFP) creates a white/purple color (arrow), and the merge of WT1 and RFP creates a yellow color. (C) In FSGS mice given enalapril, the number of Ki67 cells (C1) increased in WT1 stained cells (C2) that overlap with RFP (C3). The merge of 3 colors creates a white/purple color (arrow), and the increase in yellow reflects increased WT1 in RFP cells.

(D-F) *RenWt1<sup>fl/fl</sup>* mice. (D) At baseline, Ki67 cells are detected in tubules (arrow), but not in the JGC (D1). WT1 (D2) is not present in RFP<sup>+</sup> cells (D3). (E) At D28, neither Ki67 (E1) nor WT1 (E2) are detected in RFP cells (E3). (F) In FSGS mice given enalapril, Ki67 was restricted to the tubules (arrow) but not the JGC (F1). WT1 (F2) is not detected in RFP cells (F3). Scale bars represent 20  $\mu$ m.

## Supplemental Experimental Procedures

### **RenCreER tdTomato Wt1<sup>fl/fl</sup> reporter mice**

Ren1cCreERxRs-tdTomato-R mouse (described previously) (Pippin et al., 2013) were crossed with a *Wt1* conditional knockout mouse strain (*Wt1<sup>fl/fl</sup>*) (Martinez-Estrada et al., 2010). *Wt1* was inactivated in *RenCreER tdTomato Wt1<sup>fl/fl</sup>* mice (abbreviated *RenWt1*) by administration of 100 mg/kg tamoxifen on four occasions. The genotype of animals was identified by PCR. PCR conditions and primer sequences have been described previously (Martinez-Estrada et al., 2010). Mice were then given a tamoxifen washout period of 4 weeks, to allow it to complete exit the body and make certain no new Ren1c-creER expressing cells were labeled prior to the initiation of experiments.

Survival kidney biopsies were performed to ensure and assess CoRL labeling. Briefly, mice were anesthetized with isoflurane, and checked for depth of anesthesia via toe pinch. When the mouse is no longer responsive to external stimuli, hair is removed from the area above the kidney using clippers. Skin around the site of the incision will be disinfected using aseptic technique, on a sterile field above a circulating water heat pad. An incision is made on the flank about (1.0 cm behind the ribs and about 0.5cm below the major back muscles in mice). A sterile drape with an opening exposing the surgical site is placed over the incision site. The kidney, renal artery and renal vein are exposed through the incision. A micro-vessel clamp is placed on the renal artery and vein to reduce blood flow during biopsy (duration 1 minute). A small piece of kidney (0.4 x 0.2mm) is removed with a sharp scalpel blade. Immediately following, a piece of sterile Gelfoam (hemostatic gelatin sponge) is placed on the kidney to prevent bleeding at the biopsy site. The micro-vessel clamp is removed and kidney is checked to make certain there is no bleeding before repositioning back into the body cavity. The peritoneum and muscle will be sutured together with polyglycolic acid absorbable sutures and the skin opening closed with non-absorbable sutures or surgical clips. The

wound will be cleaned again. The mouse will be allowed to recover, under observation, on a heated pad until ambulatory. Buprenorphine is given 30 minutes pre surgery and given post-surgery to maintain pain management for at least 72 hours *RenWt1<sup>fl/fl</sup>* and *RenWt1<sup>+/+</sup>* were housed in the animal care facility of the University of Washington under specific pathogen-free conditions with food and water available ad libitum. These studies were reviewed and approved by the University of Washington Institutional Animal Care and Use Committee (2968-04)

### **Experimental models of glomerular disease accompanied by podocyte depletion**

The following experimental models of podocyte depletion were used for study:

**(i) Experimental FSGS in *RenWt1<sup>fl/fl</sup>* and *RenWt1<sup>+/+</sup>* mice:** Podocyte number was abruptly depleted in *RenWt1<sup>fl/fl</sup>* and *RenWt1<sup>+/+</sup>* mice with a cytotoxic sheep anti-glomerular antibody as previously described (Kaverina et al., 2016, Lichtnekert et al., 2016). On day three of disease, when podocyte number is decreased by 30-40% from baseline, mice were randomized into two groups; group 1 received drinking water (the vehicle for Enalapril); group 2 received the ACE-inhibitor Enalapril (75 mg/ml), refreshed weekly. Mice were sacrificed on day 28. Urine was collected at baseline, day7, day 14 and day 28. BrdU (5-bromo-2'-deoxyuridine and 5-fluoro-2'-deoxyuridine) was administered to quantitate cell proliferation as previously described (Kaverina et al., 2016).

**(ii) Podocyte TGF $\beta$  - Receptor1 transgenic (*PodTgfr1*) mice:** Podocyte number is depleted in *PodTgfr1* by doxycycline induced TGF $\beta$ 1 signaling specifically in podocytes. Progressive podocyte apoptosis leads to ~25% depletion in podocytes by day 7 and ~40% by day 14, accompanied by segmental and global glomerulosclerosis (Daehn et al., 2014).

**(iii) Passive Heymann nephritis (PHN) model of membranous nephropathy:** The (PHN) model of experimental membranous nephropathy was induced in male Sprague-Dawley rats (Charles River, Wilmington, MA) weighing 180 to 200 g by intraperitoneal injection of sheep antibody to Fx1A (5 mL/kg body weight) as previously described (Ohse et al., 2010) . Podocyte depletion has been characterized in the PHN model (Petermann et al., 2003).

**(iv) Uninephrectomy model:** The uninephrectomy model served as a negative control for podocyte depletion (Pippin et al., 2015). Following tamoxifen administration and washout, in *RenWt1<sup>+/+</sup>* as described above, kidney mass was reduced surgically. Mice were anesthetized, the left renal artery and vein were exposed through an incision and ligated with silk suture. The kidney capsule was removed from the kidney and remained along with the adrenal gland, while the left kidney itself was removed. Following recovery, the remaining right kidney was removed 12 weeks later.

### **BrdU labeling of mice to assess proliferation**

BrdU (5-bromo-2'-deoxyuridine and 5-fluoro-2'-deoxyuridine) was administered to quantitate cell proliferation. All animal groups, received BrdU 10 $\mu$ l per gram body weight (BrdU-Amersham Cell Proliferation Labeling Reagent, GE Healthcare Life Sciences, Pittsburgh, PA, RPN 202). Administration began the day after the last dose of anti-glomerular antibody was administered and was administered every 48 hours until sacrifice.

### **Laser Capture Microscopy (LCM) and quantitative reverse transcriptase polymerase chain reaction**

(qRT-PCR) To ensure *Wt1* deletion from CoRL, frozen kidney sections (10 $\mu$ m) from *RenWt1<sup>+/+</sup>* and *RenWt1<sup>fl/fl</sup>* samples were placed on positively charged glass slides. To isolate cells of renin lineage LCM was then performed as described (Tretiakova et al., 2011) with the Leica Laser Microdissection Systems LMD6500 & LMD7000 (Leica Microsystems Inc., Buffalo Grove, IL). An average of 100 to 300 cells per LCM cap were obtained from each sample and immediately subjected to complementary DNA (cDNA) synthesis and PCR. Total RNA was extracted using RNeasy Mini Kit (QIAGEN, Germantown, MD). Complementary DNA (cDNA) was synthesized using iScript cDNA Synthesis Kit (Bio-Rad, Hercules, CA). qRT-PCR assay was performed using an 7900 HT Sequence Detection System (Applied Biosystems, Foster City, CA) and iTaq SYBR Green Supermix with ROX (Bio-Rad, Hercules, CA). The thermocycling conditions consisted of denaturation at 95°C for 2.5 minutes, followed by cycles of 95°C for 15 seconds and amplification at 58°C for 30 seconds. A single PCR product of the expected size was verified by agarose gel electrophoresis. The primer sequences used were as follows: 18S forward TAGAGGGACAAGTGGCGTTC, 18S reverse CGCTGAGCCAGTCAGTGT, Ren1 forward GGAGGAAGTGGTCTCTGTCTACTACA, Ren1 reverse GCTACCTCCTAGCACACCTC, *Wt1* forward CCAGCTCAGTGAAATGGACA, *Wt1* reverse CTGTACTGGGCACCACAGAG (Figure S1C).

### **Immunoperoxidase staining**

Formalin fixed paraffin embedded mouse kidney sections (4 $\mu$ m thick) were deparaffinized in HistoClear, rehydrated in graded alcohol, and washed in phosphate buffered saline. The sections were boiled in 10mM citric acid buffer pH 6.0. and cooled for 30 minutes. Next, endogenous peroxidase activity was quenched with 3% hydrogen peroxidase solution and to block nonspecific reactions, sections were immersed in 5% milk solution for 20 minutes at room temperature. The following primary antibodies were applied on murine tissue: rabbit anti-p57 (Santa Cruz Biotechnology, Santa Cruz, CA, USA, sc-56341), rabbit anti-Cre-recombinase (Cell Signaling Technology, Danvers, MA, USA, 15036P). A horseradish peroxidase conjugated anti-rabbit polymer (Jackson Immunoresearch Laboratories, West, PA, USA, 111-001-003) was used to detect the primary antibodies. Sections were incubated with diaminobenzidine as a chromogen for 5 minutes, washed in water, and counterstained with hematoxylin. In some cases, Periodic acid Schiff's (PAS) staining was performed as a counterstain. Slides were dehydrated in ethanol and mounted with HistoMount. Reactivity was judged positive only when distinct nuclear (p57) or cytoplasmic (anti-Cre-recombinase) staining was identified.

### **Multicolor immunofluorescent staining**

Paraffin embedded mouse kidney sections (4 $\mu$ m thick) sections were used for staining. Deparaffinization, antigen retrieval and Avidin/Biotin blocking was performed as previously described (Lichtnekert et al., 2016). To identify podocytes, we used the following primary antibodies: rabbit anti-WT1 (Spring Bioscience, Pleasanton, CA, USA, E3990), rabbit anti-Podocin (Abcam, Cambridge, MA, USA, ab50339), mouse antibody to synaptopodin (Fitzgerald Industries International. Inc., Concord, MA, USA, 10R-S125a). The appropriate biotinylated secondary antibody (Vector Laboratories) was applied followed by Streptavidin, AlexaFluor 488 conjugate (Life Technologies

- Molecular Probes, Grand Island, NY, USA, S-32354). To demarcate the glomerular compartment we stained slides with collagen IV (Southern Biotechnology, Birmingham, AL, USA, 1340-08), followed by Alexa647 conjugated donkey anti-rabbit IgG (Jackson ImmunoResearch Laboratories, West Grove, PA, USA, 711-605). Biotinylated anti-renin antibody (Innovative Research Novi, ISASPREN-GF-BIO), followed by Alexa 594 conjugated streptavidin (Life Technologies, S-32356) was applied to detect renin expression. To identify CoRL we used anti-RFP antibody (Dylite 594 conjugated RFP, Rockland Immunochemicals for Research, PA, 600-401-379). For all staining, omission of the primary antibody served as a negative control.

### **Immunostaining of CoRL and MET-markers**

Paraffin embedded kidney sections (4µm) were used for staining. After performing deparaffinization, antigen retrieval and Avidin/Biotin blocking was performed as previously described (Lichtnekert et al., 2016). Antibodies were used to detect the following mesenchymal markers: αSMA (Sigma, Saint Louis, MI, USA, A2547), MYH11 (Abcam, Cambridge, MA, USA, ab53219), SM22 (Abcam, Cambridge, MA, USA, ab28811), NG2 (EMD Millipore Massachusetts, USA, AB5320). To identify epithelial cells, we used antibodies to the following markers: cytokeratin 18 (Bioss, Woburn, MA, USA, bs-2043R), E-cadherin (Cell Signaling, Danvers, MA, USA, 3195). Staining was detected with biotinylated mouse anti-rabbit IgG (Jackson ImmunoResearch) and visualized with Alexa488 conjugated streptavidin (Life Technologies). To prevent nonspecific staining for the primary antibodies from the same species pre-incubation with ChromePure rabbit IgG, Fab fragment (1:25; Jackson ImmunoResearch Laboratories, West Grove, PA, USA, 111-007) was followed by rabbit IgG Fab incubation (1:25; Jackson ImmunoResearch Laboratories, 111-003).

To identify CoRL, anti-RFP antibody (Dylite 594 conjugated RFP, Rockland Immunochemicals for Research, PA, 600-401-379) was used.

### **Triple staining of CoRL, WT1 and markers of proliferation**

In order to check for proliferation of CoRL in experimental FSGS, we used the following antibodies: mouse anti-BrdU (Biocare Medical, Concord, UK, ACR3042) or rabbit anti-Ki67 (Abcam, Cambridge, MA, USA, ab15580) followed by appropriate biotinylated secondary antibody (Vector Laboratories). The signal was amplified by incubation with streptavidin conjugated with Alexa Fluor 647 (Invitrogen, Grand Island, NY, USA). To detect CoRL, anti-RFP antibody (Dylite 594 conjugated RFP, Rockland Immunochemicals for Research, PA, 600-401-379) was applied. To detect expression of WT1 we used primary rabbit anti-WT1 (Spring Bioscience, Pleasanton, CA, USA, E3990), followed by Alexa488 conjugated donkey anti-rabbit IgG (Jackson ImmunoResearch Laboratories, West Grove, PA, USA, 711-545).

### **Urine Collection, Urine Albumin Assay, Urine Creatinine Assay**

Spot urine was collected at baseline, day 7, day 14 and day 28. Urine albumin was measured by radial immunodiffusion assay. Rabbit anti-mouse albumin antibody at 1:75 dilution (Accurate Chemical, Westbury, NY) and 4% rabbit serum (Pel-Freez, Rogers, AR) were incorporated into a thin layer of 1.5% type I, low EEO agarose

gel (Sigma-Aldrich) in 0.5 M veronal buffer, poured into Integrid 100x15 mm square petri dish on a leveling platform (VWR, West Chester, PA). Urine was placed in a well cut into the agar layer. As the antigens diffuse from the well, only the specific antigen (albumin) reacted with its antibody in the agar. The reaction formed a halo of precipitation around the well. A measurement of the halo after it had reached maximal size was related directly to antigen concentration, with reference made to a calibration curve prepared from known concentrations of purified fraction V mouse albumin standards (MP Biomedicals, Irvine, CA) tested under identical conditions. Creatinine was measured in the urine via a colorimetric assay according to the manufacturers instructions (Cayman Chemical, Ann Arbor, MI) and an albumin to creatinine ratio was calculated.

### **Confocal Microscopy**

Images were obtained on Leica TCS SPE II laser scanning confocal microscope. Multi-color immunofluorescent images were collected at 200x and 400x magnification and a high 1.2 NA oil-immersion objective. Images were acquired in original Tagged Image Format File, with a bit depth of 15, no binning, and a total size of 512x512 pixels with each pixel corresponding to 0.27  $\mu\text{m}$ . Each antibody staining was adjusted for background correction. Appropriate single stained controls were used with each antibody to check that there was no fluorochrome cross-bleeding.

### **Human biopsies of glomerular disease**

In order to determine if the expression pattern for WT1 in renin expressing cells seen under experimental conditions was recapitulated in human disease, paraffin-embedded kidney biopsies from patients with FSGS, not otherwise specified (n=10) and Membranous nephropathy (n=10) were obtained from the University of Chicago. Normal human kidney paraffin-embedded sections were used as controls. The study protocol was approved by the University of Chicago Institutional Review Board. For double immunostaining of WT1 and renin, 4 $\mu\text{m}$  thick kidney sections were stained with immunofluorescent antibodies against WT1 (Spring Bioscience, Pleasanton, CA, USA) followed by Alexa488 conjugated donkey anti-rabbit IgG (Jackson ImmunoResearch Laboratories, West Grove, PA, USA) and biotinylated anti-renin antibody (LifeSpan Bioscience, Seattle, WA, USA), followed by Alexa 594 conjugated streptavidin (Life Technologies). Appropriate single stained controls were used with each antibody to ensure no fluorochrome cross-reactivity; omitting the primary antibodies served as negative controls.

### **Supplemental References**

Daehn, I., G. Casalena, T. Zhang, S. Shi, F. Fenninger, N. Barasch, L. Yu, V. D'Agati, D. Schlondorff, W. Kriz, B. Haraldsson and E. P. Bottinger (2014). Endothelial mitochondrial oxidative stress determines podocyte depletion in segmental glomerulosclerosis. *J Clin Invest* 124, 1608-1621. Kaverina, N. V., D. G. Eng, R. R. Schneider, J. W. Pippin and S. J. Shankland (2016). Partial podocyte replenishment in experimental FSGS derives from nonpodocyte sources. *Am J Physiol Renal Physiol* 310, F1397-1413. Lichtnekert, J., N. V. Kaverina, D. G. Eng, K. W. Gross, J. N. Kutz, J. W. Pippin and S. J. Shankland (2016). ReninAngiotensin-Aldosterone System Inhibition Increases

Podocyte Derivation from Cells of Renin Lineage. *J Am Soc Nephrol*. Martinez-Estrada, O. M., L. A. Lettice, A. Essafi, J. A. Guadix, J. Slight, V. Velecela, E. Hall, J. Reichmann, P. S. Devenney, P. Hohenstein, N. Hosen, R. E. Hill, R. Munoz-Chapuli and N. D. Hastie (2010). WT1 is required for cardiovascular progenitor cell formation through transcriptional control of Snail and E-cadherin. *Nat Genet* 42, 899-903. Ohse, T., M. R. Vaughan, J. B. Kopp, R. D. Krofft, C. B. Marshall, A. M. Chang, K. L. Hudkins, C. E. Alpers, J. W. Pippin and S. J. Shankland (2010). De novo expression of podocyte proteins in parietal epithelial cells during experimental glomerular disease. *Am J Physiol Renal Physiol* 298, F702-711. Petermann, A. T., R. Krofft, M. Blonski, K. Hiromura, M. Vaughn, R. Pichler, S. Griffin, T. Wada, J. Pippin, R. Durvasula and S. J. Shankland (2003). Podocytes that detach in experimental membranous nephropathy are viable. *Kidney Int* 64, 1222-1231. Pippin, J. W., N. V. Kaverina, D. G. Eng, R. D. Krofft, S. T. Glenn, J. S. Duffield, K. W. Gross and S. J. Shankland (2015). Cells of renin lineage are adult pluripotent progenitors in experimental glomerular disease. *Am J Physiol Renal Physiol* 309, F341-358. Pippin, J. W., M. A. Sparks, S. T. Glenn, S. Buitrago, T. M. Coffman, J. S. Duffield, K. W. Gross and S. J. Shankland (2013). Cells of renin lineage are progenitors of podocytes and parietal epithelial cells in experimental glomerular disease. *Am J Pathol* 183, 542-557. Tretiakova, M. and J. Hart (2011). Laser microdissection for gene expression study of hepatocellular carcinomas arising in cirrhotic and non-cirrhotic livers. *Methods Mol Biol* 755, 233-244. Zhang, J., D. Yanez, A. Floege, J. Lichtnekert, R. D. Krofft, Z. H. Liu, J. W. Pippin and S. J. Shankland (2015). ACE inhibition increases podocyte number in experimental glomerular disease independent of proliferation. *J Renin Angiotensin Aldosterone Syst* 16, 234-248.